PURDUE UNIVERSITY
GRADUATE SCHOOL
Thesis/Dissertation Acceptance

This is to certify that the thesis/dissertation prepared

By Pin Li

Entitled Effects of Carbon Nanotubes on Airway Epithelial Cells and Model Lipid Bilayers: Proteomic and Biophysical Studies

For the degree of Master of Science

Is approved by the final examining committee:

Dr. Bonnie Blazer-Yost

Dr. Frank Witzmann

Dr. Stephen Randall

Dr. Horia Petrache

To the best of my knowledge and as understood by the student in the *Thesis/Dissertation Agreement. Publication Delay, and Certification/Disclaimer (Graduate School Form 32)*, this thesis/dissertation adheres to the provisions of Purdue University's "Policy on Integrity in Research" and the use of copyrighted material.

Bonnie L. Blazer-Yost

Approved by Major Professor(s): _____

_____

Approved by: Xianzhong Wang 04/02/2014

Head of the Department Graduate Program Date

EFFECTS OF CARBON NANOTUBES ON AIRWAY EPITHELIAL CELLS AND MODEL LIPID BILAYERS: PROTEOMIC AND BIOPHYSICAL STUDIES

A Thesis

Submitted to the Faculty

of

Purdue University

by

Pin Li

In Partial Fulfillment of the

Requirements for the Degree

of

Master of Science

August 2014

Purdue University

Indianapolis, Indiana

I would like to dedicate this thesis to my parents, from whom I have got unconditional love and support and inherited the great curiosity and passion for learning...

ACKNOWLEDGEMENTS

First of all, I would like to express my heart-felt thanks to my mentor, Dr. Bonnie Blazer-Yost. It was extremely fortunate for me to have such a mentor, who always had time for me, and taught me so much in every aspect of science, from experimental design to data analysis, from critical thinking to scientific writing. I admire her knowledge and her personality.

Then I would also like to express my gratitude to my committee members: Dr. Frank Witzmann, Dr. Horia I. Petrache and Dr. Stephen Randall, who have offered me constant help, invaluable advice and informative suggestions. My sincere thanks also go to Dr. Robert Yost and the Bonnie Blazer-Yost (BBY) laboratory team (past and present): Shanta Lewis, M.S., Stephanie Flaig, M.S., Gabriel Martinez, and Ellen Maue. Many thanks to the Department of Biology faculty and staff, the School of Science and Indiana University-Purdue University Indianapolis for this once in a life time opportunity.

Last but not least, I would like to express my thanks to my family and my friends for their valuable encouragement and spiritual support during my study.

TABLE OF CONTENTS

Page

LIST OF ABBREVIATIONS

Calu-3	Cultured Human Airway Epithelial Cells
CFTR	Cystic fibrosis transmembrane conductance regulator
CNT	Carbon nanotube
d.nm	Diameter in nanometer
DPhPC	1, 2-diphytanoyl-sn-glycero-3-phosphocholine
FBS	Fetal bovine serum
gA	Gramicidin A
IPA	Ingenuity Pathway Analysis
KCl	Potassium chloride
LFQMS	Label-free quantitative mass spectrometry
M	Mole (Unit)
ms	Millisecond
MWCNT	Multi-wall carbon nanotube
STRING	Search Tool for the Retrieval of Interacting Genes
SWCNT	Single-wall carbon nanotube
TEER	Trans epithelial electric resistance

ABSTRACT

Li, Pin. M.S., Purdue University, August 2014. Effects of Carbon Nanotubes on Airway Epithelial Cells and Model Lipid Bilayers: Proteomic and Biophysical Studies. Major Professor: Bonnie L. Blazer-Yost.

Carbon nanomaterials are widely produced and used in industry, medicine and scientific research. To examine the impact of exposure to nanoparticles on human health, the human airway epithelial cell line, Calu-3, was used to evaluate changes in the cellular proteome that could account for alterations in cellular function of airway epithelia after 24 h exposure to 10 μg/mL and 100 ng/mL of two common carbon nanoparticles, single- and multi-wall carbon nanotubes (SWCNT, MWCNT). After exposure to the nanoparticles, label-free quantitative mass spectrometry (LFQMS) was used to study differential protein expression. Ingenuity Pathway Analysis (IPA) was used to conduct a bioinformatics analysis of proteins identified by LFQMS. Interestingly, after exposure to a high concentration (10 μg/mL; 0.4 μg/cm2) of MWCNT or SWCNT, only 8 and 13 proteins, respectively, exhibited changes in abundance. In contrast, the abundance of hundreds of proteins was altered in response to a low concentration (100 ng/mL; 4 ng/cm2) of either CNT. Of the 281 and 282 proteins that were significantly altered in response to MWCNT or SWCNT, respectively, 231 proteins were the same. Bioinformatic analyses found that the proteins common to both kinds of nanotubes are associated with the cellular functions of cell death and survival, cell-to-cell signaling and

interaction, cellular assembly and organization, cellular growth and proliferation, infectious disease, molecular transport and protein synthesis. The decrease in expression of the majority proteins suggests a general stress response to protect cells. The STRING database was used to analyze the various functional protein networks. Interestingly, some proteins like cadherin 1 (CDH1), signal transducer and activator of transcription 1 (STAT1), junction plakoglobin (JUP), and apoptosis-associated speck-like protein containing a CARD (PYCARD), appear in several functional categories and tend to be in the center of the networks. This central positioning suggests they may play important roles in multiple cellular functions and activities that are altered in response to carbon nanotube exposure.

To examine the effect of nanotubes on the plasma membrane, we investigated the interaction of short purified MWCNT with model lipid membranes using a planar bilayer workstation. Bilayer lipid membranes were synthesized using neutral 1, 2-diphytanoyl-sn-glycero-3-phosphocholine (DPhPC) in 1 M KCl. The ion channel model protein, Gramicidin A (gA), was incorporated into the bilayers and used to measure the effect of MWCNT on ion transport. The opening and closing of ion channels, amplitude of current, and open probability and lifetime of ion channels were measured and analyzed by Clampfit. The presence of an intermediate concentration of MWCNT (2 μg/ml) could be related to a statistically significant decrease of the open probability and lifetime of gA channels.

The proteomic studies revealed changes in response to CNT exposure. An analysis of the changes using multiple databases revealed alterations in pathways, which were consistent with the physiological changes that were observed in cultured cells exposed to

very low concentrations of CNT. The physiological changes included the break down of the barrier function and the inhibition of the mucocillary clearance, both of which could increase the risk of CNT's toxicity to human health. The biophysical studies indicate MWCNTs have an effect on single channel kinetics of Gramicidin A model cation channel. These changes are consistent with the inhibitory effect of nanoparticles on hormone stimulated transepithelial ion flux, but additional experiments will be necessary to substantiate this correlation.

CHAPTER 1. INTRODUCTION

1.1 Nanotechnology

Nanotechnology is the manipulation of matter at atomic and molecular scales from 1 to 100 nanometers in diverse fields such as physics, chemistry, biology, materials science, and engineering. After more than 20 years of basic nanoscience research, nanotechnology brings the development of new technology and the creation of new materials with wide ranging applications in information technology, energy, environmental science, medicine, homeland security, food safety, and transportation.

Using nanotechnology, materials can effectively be made to be stronger, lighter, more durable, more reactive, or better electrical conductors than the materials we use today. The special properties of nanoparticles include unique surface area/volume ratios, refractive indices, and biological and chemical reactivity, which help to extend their applications. In biomedical research, nano-technologies can provide essential breakthroughs in many fields including the fight against cancer [1]. The success of targeted delivery of nanovectors such as liposomes with anticancer drugs for the therapy of breast cancer suggests nanocarriers could be an emerging platform for cancer therapy [2]. Biologically targeted, nanosized magnetic resonance imaging (MRI) contrast agents for intraoperative imaging in the context of neuro-oncological interventions could be a new approach to delineation of brain tumors [3]. Novel, nanoparticle-based methods for

high-specificity detection of nuclear acids and proteins have been used for the early detection of precancerous tissue [4].

With the variety of potential applications from clinical treatments to research to industry and even the military, governments all over the world have invested billions of dollars in nanotechnology research. According to the 2014 Federal Budget of United States federal government, more than $1.7 billion will be provided to the National Nanotechnology Initiative (NNI), reflecting a steady growth in the NNI investment and the cumulative NNI investment since 2001 to almost $20 billion in total [5]. Through the estimation by NNI, the governments of the European Union (EU) and Japan invested approximately $1.7 billion and $950 million, respectively, in nanotechnology research and development.

While the application of nanotechnology is promising, the potential risk involved with their toxicity and environmental impact needs to be addressed and further studied [6]. Potential effects on human health are an issue in the manufacturing workplace and after environmental exposure [7]. Studies show that inhaled nanoparticles can cause lung damage, and then translocate through the circulatory, lymphatic, and nervous systems to many tissues and organs, including the brain [8]. Likewise, research into the rational delivery and targeting of nanomedicines has yielded promising results, but clearance and cell toxicity of these nanovectors are poorly understood and adverse effects on human health remain a potential problem [9].

1.2 Carbon nanotubes

One family of widely used nanomaterials is carbon nanotubes (CNTs), which was discovered by Sumio Iijima in 1991 [10]. CNTs are hollow carbon tubes made of a single or several concentrically arranged cylindrical graphite layers capped by fullerenic hemispheres (as shown in Figure 1), which are referred to as single- and multi-wall carbon nanotubes (SWCNT, MWCNT). Manufactured single-walled nanotubes can have diameter and length ranging between 0.5–3.0 nm and 20–1000 nm. While the corresponding dimensions for multi-walled nanotubes can be as large as 1.5–100 nm and 1–50 μm [9].

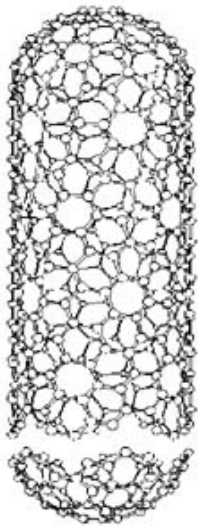

Figure 1 Structure of a typical Single Wall Carbon Nanotube. Provide by SES Research.

With high tensile strength, ultra-light weight, and excellent chemical and thermal stability as well as semi- and metallic-conductive properties, CNTs have been incorporated in many commercial applications ranging from rechargeable batteries, automotive parts, water filters, thin-film electronics and large-area coatings. The growing

commercial interest in CNTs is reflected by the production capacity of several thousand tons a year, which is still increasing [11].

In addition to many industrial applications, the dimensional and chemical compatibility of CNTs with cells and biomolecules such as DNA and proteins make it a promising biomaterial. These features have led to many proposed applications in the biomedical field, including biosensors, drug and vaccine delivery and reinforced and/or conductive polymer nanocomposites [12].

By selective recognition and binding of target proteins with specific receptors, functionalized CNTs can have a distinct change in conductance that can be detected. Combined with the sensitive nanotube electronic devices, this specific binding enables highly specific electronic sensors for biomolecules diagnostics of diseases [13]. Loaded with active molecules by forming stable covalent bonds or supramolecular assemblies based on noncovalent interactions, CNTs can get into cells by endocytosis or penetrating the lipid bilayer without causing cell death [14]. They can be used as transporting vehicles for intracellular delivery of bioactive molecules such as drug delivery, protein delivery, gene therapy and cancer therapy applications [15]. Due to their structural characteristics at the nanoscale level, 3D-MWCNT-based networks are ideal for scaffolds/matrices in tissue engineering [16]. CNTs can sustain osteoblast proliferation and bone formation, thus represent a potential nanotechnology in bone bioengineering [17].

The diversity of lengths, aspect ratios, dispersion, surface coating and functionalization of CNTs further enhances their biocompatibility and biomedical application, but also raises concerns about their potential cytotoxicity [18]. With the

needle-like fiber shape similar to asbestos, CNT could induce asbestos-like, length-dependent, pathogenic behavior including inflammation and formation of granulomas. This has been demonstrated when introduced into the abdominal cavity of mice [19]. In addition, intratracheal instillation of carbon nanotube in mice for 7 days also induced dose-dependent epithelioid granulomas and interstitial inflammation. Chronic exposure for 90 days revealed peribronchial inflammation in lungs and necrosis that had extended into the alveolar septa [20]. Further study of potential hazards and toxicity effects of this nanomaterial for human health in general as well as in professionally exposed workers is important. In addition, the environmental impact must be understood if long-term harm is to be avoided.

CHAPTER 2. EFFECTS OF CARBON NANOTUBES ON AIRWAY EPITHELIAL CELLS

2.1 CNT's effect on Airway epithelium and Calu-3 cells

A primary route for nanoparticle uptake in humans is through the airways, and high concentrations of carbon nanoparticles are known to cause oxidative stress, inflammatory responses and granuloma formation in respiratory epithelia [21]. Calu-3 is one of the airway cell lines commonly used for bronchial epithelial cell studies.The serous cells, of which Calu-3 are a model, are a major source of airway surface liquid, mucins and immunologically active substances [22]. Mucus protects the epithelium from infection and chemical damage by binding to inhaled microorganisms and particles that are subsequently removed by the mucociliary escalator system. Bronchial secretion and mucociliary clearance (MCC) are critical components of the innate immune response to remove inhaled pathogens and particulates.

The Calu-3 cells mimic the *in vivo* serous cells in that they form an epithelium that secretes a layer of mucous that covers the apical surface. An additional characteristic in common with the serous cells *in vivo* is that the Calu-3 cell line has cell junctions that serve a barrier function, protecting the internal milieu from the external milieu. Trans Epithelial Electric Resistance (TEER), which consists of paracellular and transcellular resistances, is used as a measurement of the barrier function of epithelial cells [23]. The formation of an intact, confluent cellular monolayer can be verified by an increase in

TEER. We have previously shown a decrease in TEER of confluent monolayers after exposure to CNTs for 24 or 48 h. The decrease in barrier function in response to CNT exposure was manifested after exposure to the same, low concentration (100 ng/mL) that we have used in the current studies. The magnitude of the decrease indicated a disruption of the barrier function but no loss of cellular viability [24]. In the case of cell death, the confluent monolayer would have "holes" and it would be impossible to maintain a measureable transepithelial resistance. Thus, the TEER value is a more sensitive measure of cellular viability than most biochemical assays.

The serous cells also play a role in maintaining airway hydration by selective absorption or secretion of electrolytes which is accompanied by compensatory water flux. Our previous studies showed that CNT exposure over a wide range of concentrations decreases a secretory Cl^- flux that is stimulated in response to epinephrine [24]. Since a compensatory water flux will accompany the Cl^- secretion, these results indicate a potential for CNT-induced alterations in airway hydration.

The current studies extend our previous observations to a bioinformatic analysis of changes that occur in the Calu-3 cell proteome in response to exposure to a physiologically relevant concentration of carbon nanotubes. The current results corroborate the earlier studies showing that there is an inverse dose response relationship between the concentration of carbon nanotubes and the functional effects on barrier epithelial cells [24,25]. Furthermore, the results elucidate the protein molecular basis for a variety of major functional changes in the cells. The quantification and bioinformatic analysis of protein expression changes in response to carbon nanotube exposure provides

a comprehensive understanding of the effect of carbon nanotubes on epithelial cells as well as a background for future toxicological studies.

2.2 Methods

2.2.1 Cell culture media preparation

DMEM/F-12 tissue culture media, Glutamax, penicillin, streptomycin, sodium pyruvate, and non-essential amino-acids were purchased from Invitrogen (Carlsbad, CA, USA). Fetal bovine serum (FBS) was from Gemini Bioproducts, (West Sacramento, CA, USA). Cell culture flasks and Transwellcell culture plates (24 mm inserts, polycarbonate, 0.4 μm pore size) were obtained from Costar-Corning (Acton, MA, USA). DL-Dithiothreitol (DTT), urea, triethylphosphine, iodoethanol, and ammonium bicarbonate were purchased from Sigma-Aldrich (St. Louis, MO, USA). LC-MS grade 0.1% formic acid in acetonitrile and 0.1% formic acid in water were purchased from Burdick & Jackson (Muskegon, MI, USA). Modified sequencing grade porcine trypsin was obtained from Princeton Separations (Freehold, NJ, USA).

2.2.2 Carbon nanotube preparation

CNTs were purchased from SES Research (Houston, TX, USA). Based on the manufacturer's data, SWCNT (#900-1301) (long) were purified single-walled nanotubes with an outer diameter <2 nm and lengths ranging from 5–15 μm. The purity was reported to be >90%CNT (>50% SWCNT) containing ash (<2% wt) and amorphous carbon (<5% wt). Purified MWCNT (# 900-1203) had a reported outer diameter of 40–60

nm with lengths ranging from 5–15 μm. The MWCNT were reported to be >95% nanotubes with low level of amorphous carbon (<2%), and ash content (<0.2%).

Concentrated stock solutions of SWCNT and MWCNT were prepared by sonication in FBS at a concentration of 5 mg/mL using a Branson Sonicater 450 at a duty cycle of 30% and an output control of 3 for 20 s. After sonication, the samples were autoclaved and diluted to the final concentrations of nanoparticles in the cell culture media. For the control samples, FBS without nanoparticles was treated in an identical manner. Additional CNT-free FBS was added to obtain a final concentration of 15% FBS in culture media in all cases. Only 2% of the total FBS was autoclaved with CNTs.

2.2.3 Cell culture and incubation

The Calu-3 (ATCC No. HTB-55) cell line was purchased from American Type Culture Collection (Manassas, VA, USA) at passage 19. Cells were grown in humidified atmosphere of 5% CO2–95% air at 37°C. Cell culture medium was comprised of DMEM/F-12 (1:1), 15% FBS, 2.40 mg/L NaHCO3, 100 U/L penicillin, 100 mg/L streptomycin, 0.5 mM sodium pyruvate, 0.5 mM non-essential amino acids, and 1 mMGlutamax. All cultures had media replaced thrice weekly.

Cells maintained and amplified in plastic tissue culture plates were trypsinized and seeded directly onto the permeable filters of the Transwell cell culture inserts with media on the apical and basolateral sides. Two days after inoculation, the medium was removed from both sides and replaced only on the basolateral side. This cell culture technique, called air interface culture (AIC), mimics the *in vivo* situation. The Calu-3 cells secrete a sufficient amount of fluid and mucus to remain hydrated. Cell monolayers were used on

days 12–14 after being seeded on the Transwells, the time at which the cells form confluent, electrically tight monolayers with tight junctions and show a high resistance phenotype.

The CNTs, at concentrations of 10 μg/mL and 100 ng/mL, were added to the apical media and cells were exposed for 24 h. Only 200 μL of CNT containing media were added to the apical side (5 cm^2) to maintain the AIC for the cells. However, all volumes were maintained in constant proportions so that the surface exposure could be converted to concentration per unit volume of media using the following formula: N g/cm^2 = 25N g/mL. Therefore, the concentrations used in the experiments could also be expressed as 0.4μg/cm^2 and 4 ng/cm^2 respectively.

2.2.4 Label-Free Quantitative Mass Spectrometry

After exposure to CNT for 24h, label-free quantitative mass spectrometry (LFQMS) was applied to examine differential protein expression in cell lysates by Dr. Witzmann and Dr. Lai from Proteomics Core in Indiana University School of Medicine, as published previously [26-29]. The Transwell™ membranes containing adherent Calu-3 cells were rinsed 3 times in ice-cold 250 mM sucrose, snap frozen in liquid nitrogen, and stored at −80 °C. Calu-3 lysates were prepared by adding 500 μL of lysis buffer (8 M urea, 10 mM DTT, freshly prepared) to each sample. Cells were incubated at 35 °C for 1 h with agitation and then centrifuged at 15,000 ×g for 20 min at 4 °C to remove insoluble materials. The fully solubilized cell proteins in the supernatant were then stored at −80 °C until LFQMS analysis.

Protein concentration was determined by the Bradford Protein Assay using Bio-Rad (Hercules, CA, USA) protein assay dye reagent concentrate. An aliquot containing 100 μg of each cell lysate sample was adjusted to 200 μL with 4 M urea and then reduced and alkylated by triethylphosphine and iodoethanol, as described previously [30]. A 150 μL aliquot of a 20 μg/mL trypsin solution was added to the sample and incubated at 35 °C for 3 h, after which another 150 μL of trypsin was added, and the solution incubated at 35 °C for 3 h. Exactly 20 μg of each tryptic digest sample was injected randomly as two technical replicates onto a C18 reversed phase column (TSK gel ODS-100V, 3 μm, 1.0 mm × 150 mm) at a flow rate of 50 μL/min as part of the Surveyor autosampler and MS HPLC system (Thermo-Electron, Waltham, MA, USA) coupled to a Thermo-Finnigan linear ion-trap (LTQ) mass spectrometer. The mobile phases A and B were 0.1% formic acid in water and 50% ACN with 0.1% formic acid in water, respectively. The gradient elution profile was as follows: 10% B (90% A) for 7 min and 10%–67.1% B (90%–32.9% A) for 163 min, 67.1%–100% B (32.9%–0% A) for 10 min. The spectral data were collected in the "data dependent MS/MS" mode with the ESI interface using a normalized collision energy of 35%. Dynamic exclusion settings were repeat count 1, repeat duration 30 s, exclusion duration 120 s, and exclusion mass width 0.6 m/z (low) and 1.6 m/z (high). A blank was injected between each sample to clean and balance the column and to eliminate carryover. The acquired data were searched against the International Protein Index (IPI) database (ipi.HUMAN.v3.83) using SEQUEST (v. 28 rev. 12) algorithms in Bioworks (v. 3.3). General parameters were set to: peptide tolerance 2.0 amu, fragment ion tolerance 1.0 amu, enzyme limits set as "fully enzymatic-cleaves at both ends", and missed cleavage sites set at 2. Peptide and protein

identifications were validated by PeptideProphet [31] and ProteinProphet [32] in the Trans-Proteomic Pipeline (TPP, v. 3.3.0) [33]. Only proteins with probability ≥0.9000 and peptides with probability ≥0.8000 were reported. Protein abundance was determined using IdentiQuantXL™ [34]. Briefly, after chromatogram alignment and peptide retention time determination, a weighted mean m/z of each peptide was calculated and a tab delimited file was created to extract peptide intensity using MASIC [35]. Peptides were then filtered according to intensity CV across all samples and intensity correlation, for those identifying a particular protein. Protein abundance was calculated from all qualified corresponding peptides matched to that protein.

Comparison of the abundance of individual protein dose-group means generated by LFQMS was performed within the IdentiQuantXL™ platform using one-way ANOVA and Pairwise Multiple Comparisons (Holm-Sidak method). Critical F-ratio significance for ANOVA was set at $p < 0.01$ and pairwise comparison at $p < 0.05$. False Discovery Rate (FDR) [36] was estimated using Q-value software.

2.2.5 Ingenuity Pathway Analysis

Protein lists and their corresponding expression values (fold change) were imported into the Ingenuity Pathway Analysis (IPA) web based software [37] to interpret the biological relevance of the differential protein expression data. IPA Core Analysis was used to get a rapid assessment of the signaling and metabolic pathways, upstream regulators, molecular networks, and biological processes. IPA Functional Analysis was identified based on Ingenuity Pathway Knowledge Base (IPKB) that was most significantly related to the dataset. p-value calculated by Right-tailed Fisher's exact test

was used to determine the probability that each biological function assigned to that data set was due to chance alone. The Canonical Pathways Analysis identified the pathways from IPA's library of canonical pathways based on the proteins involved in each pathway. The Upstream Regulator Analytic identified the cascade of upstream transcriptional regulators that can explain the observed gene expression changes in a dataset and illuminate the biological activities occurring in the tissues or cells being studied.

R language was used to compare the biological effects across different CNTs and exposure levels. Proteins involved top biological functions of exposure to high concentrations of SWCNT and MWCNT were compared in Venn diagrams.

2.2.6 String database analysis

Search Tool for the Retrieval of Interacting Genes (STRING) database was used to analyze the proteins involved in each function and predict protein interaction networks. STRING [38] is a database and web resource dedicated to protein-protein interactions, including both direct (physical) and indirect (functional) associations [39]. It weights and integrates information from numerous sources, including high-throughput experimental data, the mining of databases and literature, and predictions based on genomic context analysis. STRING integrates and ranks these associations by benchmarking them against a common reference set, and presents evidence in a consistent and intuitive web interface as a network. Interactions in STRING are provided with a confidence score, and accessory information such as protein domains and 3D structures is made available, all within a stable and consistent identifier space.

2.3 Results and Discussion

2.3.1 Proteomics

LFQMS identified and quantified 2,852 unique protein database entries in the Calu-3 cell line. Statistical analysis by ANOVA ($p < 0.01$) and Pairwise Multiple Comparisons ($p < 0.05$) determined that incubation with CNT at concentrations of 10 μg/mL and 100ng/mL resulted in significant changes in protein expression profiles (Figure 2). Volcano plots in Figure 3 show the log2 fold change and *p*-value of all proteins in treated compared with untreated, control cultures. At the high concentration, the volcano plot tends to be symmetrical, which indicates the exposure to high concentration of CNTs caused comparable increases and decreases in protein expression. Additionally, the expression of few proteins was significantly different ($p < 0.05$). Conversely, at the low concentration, the abundance of many proteins was significantly changed and the volcano plot is skewed to the left, indicating that the relative amount of a majority of the proteins was decreased after CNT exposure. Among all the exposures, only 3, 2, 1, 1 proteins had increased expression at concentration of 10 μg/mL MWCNT, 10 μg/mL SWCNT, 100 ng/mL MWCNT, 100 ng/mL SWCNT, respectively. After exposure to high concentration of MWCNT and SWCNT, only 8 and 13 proteins significantly changed, while after exposure to low concentration of MWCNT and SWCNT, the abundance of 283 and 282 proteins was significantly altered.

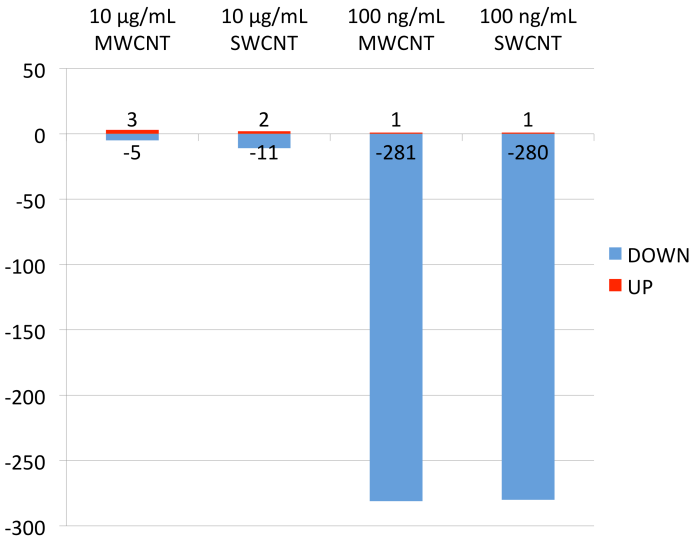

Figure 2 Changes in protein abundance in response to carbon nanotube exposure. The bars depict the number of proteins whose expression was increased (above 0) or decreased (below 0) over controls in response to 24 h exposure to carbon nanotubes at the concentrations listed on the figure. Actual numbers of proteins whose abundance are altered are also shown on the graph. Protein expression data filtered by ANOVA $p < 0.01$ and Pairwise Multiple Comparison $p < 0.05$ of different CNTs (SWCNT, MWCNT) and concentrations (10 µg/mL, 100 ng/mL).

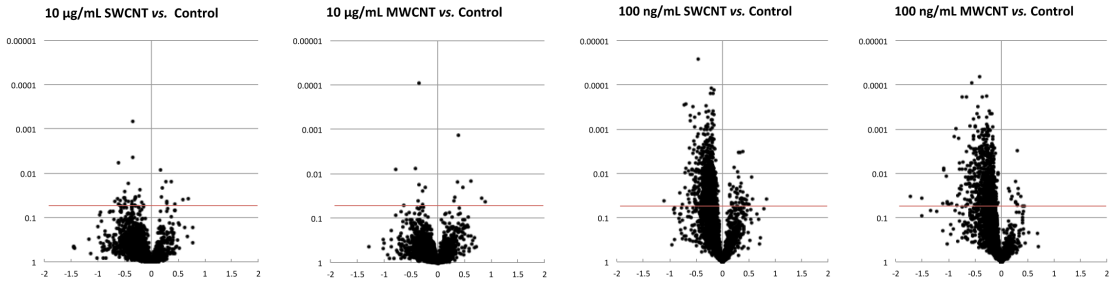

Figure 3 Volcano plots of all proteins identified and quantified, illustrating their magnitude, significance, and direction of differential expression observed after 24 h exposure to CNTs (SWCNT, MWCNT) at two different concentrations, 10 µg/mL, 100 ng/mL. The horizontal red line in each graph signifies Pairwise Multiple Comparisons p-value < 0.05 compared to proteins in control cultures grown in parallel.

These findings are consistent with our previous studies showing that 24 h exposure to the high concentration (10 µg/mL) has little effect on cell function measured as TEER.

Conversely the lower concentration of CNTs (100 ng/mL) caused an approximately 40% decrease in TEER [24]. These results are also consistent with studies performed on high resistance renal epithelial cells where both TEER and hormone-stimulated ion transport showed an inverse relationship between CNT concentration and functional effect [25]. We hypothesize that the difference in effect between the high and low dose CNT exposure could be due to the propensity of carbon nanotubes to agglomerate at high concentration. This postulate is supported by analysis of particle size and zeta potential of nanoparticles in previous research in our laboratory [24,25]. At the high concentrations, the nanoparticle agglomerates are very large and are unlikely to cross the cell membrane to alter cellular function [25]. However at lower concentrations these large aggregates are not present. A previous *in vivo* study showed that small agglomerated groups of nanoparticles can be readily phagocytized by alveolar macrophages while single nanoparticles can have a higher probability of translocating to the circulatory system and organs where they can produce damage [40]. In addition, at the low concentrations, the CNTs are better dispersed, and can competitively bind to serum proteins. Nanoparticle/serum protein complex formation alters their adsorption capacity and packing modes [41].

Transmission electron microscopy (TEM) analysis of CNTs in cell culture medium support protein coating of nanoparticles (data not shown). Liquid chromatography-tandem mass spectrometry found the CNTs associate with proteins forming a protein corona after incubation with PBS-DMEM cell culture media [42]. It is the nanoparticle-corona complex, rather than the bare nanoparticle, that can interact with biological machinery [43]. The protein-coated CNTs may activate the cell's uptake machinery in a

process known as endocytosis, which may enable the CNTs to enter the cell through cell membrane and even the nucleus [44].

The Venn Diagram shown in Figure 4 compares the individual protein changes and their overlap among all of the nanoparticle exposures. There was no overlap in four categories, which means there were no proteins that changed in all exposures. There is a protein, EPRS, found to have a decrease in expression in response to low concentration exposure of SWCNT and MWCNT as well as low concentration of SWCNT. It is a kind of bifunctional aminoacyl-tRNA synthetase that is involved in protein biosynthesis and translation regulation [45]. Clearly, the low concentration (100 ng/mL) showed the highest number of changes and a remarkable overlap between MWCNT and SWCNT. Between the 281 and 282 proteins that had significant fold changes in MWCNT and SWCNT, 231 proteins were the same. At the high concentration, few proteins were differentially expressed, and these showed a lesser degree of overlap. There was also no overlap between the high and low concentrations of the same CNT, so it is the concentration, not the CNT itself that had the most effect on cells.

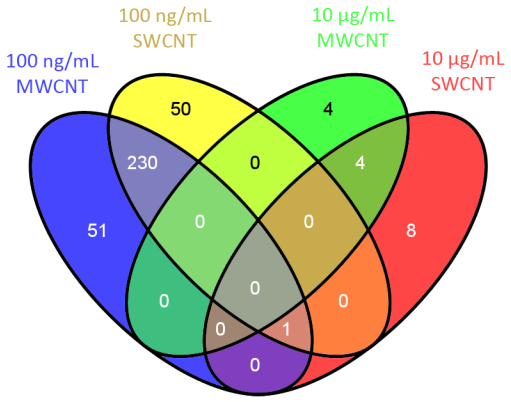

Figure 4 Venn diagram illustrating common identities of the proteins altered in response to 24 h CNT exposure. Overlaps of identical significantly altered protein expressions after exposure to two different concentrations (10 µg/mL, 100 ng/mL) of either SWCNT or MWCNT are indicated by the numbers inside each of the different compartments.

The magnitude of the CNT-induced changes in protein expression was low. Of all the increased proteins, the highest fold change was 1.3. However, decreased expression reached as high as 2.1 fold. The relatively low level of change is not surprising in light of the physiological functional changes demonstrated in previous studies [24,25]. Within the concentration range used in the current studies, CNTs decreased the barrier function of both renal and airway high resistance epithelial cell lines but did so without altering cellular viability. In the Calu-3 cells, exposure decreased, but did not fully inhibit, epinephrine stimulated Cl^- secretion. Therefore some cellular functions are altered but the CNTs are not overtly toxic so one would anticipate compensatory changed in cell metabolism manifested as modest changes in protein content.

2.3.2 Bioinformatics

After analysis by IPA, we identified proteins within several categories including top biological functions, canonical pathways and upstream regulators associated with differentially expressed proteins. Because of their small number, this analysis could not be performed for proteins altered by the high concentration exposure.

Due to the remarkable overlap of protein expression changes between MWCNT and SWCNT after the 100 ng/mL exposure, the predicted canonical pathways, upstream regulators, and biological functions were nearly identical. Within identical or similar functions, Venn Diagrams were used to demonstrate the overlap between MWCNT and SWCNT exposure (Figure 5). Some functions had different annotations assigned by the software, but they were in similar categories, so they were also compared. For example, in the only category with increased function, cell death, 40 of the 44 proteins mapped to "cell death of tumor cell lines" after exposure to MWCNT. These proteins were also part of the 87 proteins mapped to "cell death" after exposure to SWCNT. Regarding decreased function, all the five proteins in the category "quantity of intercellular junctions" were significantly decreased after exposure to either of the CNTs. Because there was so much overlap between biological activities resulting from Calu-3 cell exposure to MWCNT and SWCNT, we focused on those proteins that were differentially expressed in both exposures. IPA analysis of these 231 proteins was used to assign canonical pathways and upstream regulators significantly associated with them.

	MW		SW	
a	Cell Death Of Tumor Cell Lines	44	Cell Death	87
b	Recruitment Of Leukocytes	13	Recruitment Of Leukocytes	11
c	Quantity Of Intercellular Junctions	5	Quantity Of Intercellular Junctions	5
d	Proliferation Of Cells	93	Proliferation Of Cells	88
e	Viral Infection	49	Viral Infection	49
f	Transport Of Protein	13	Transport Of Protein	14
g	Metabolism Of Protein	34	Synthesis Of Protein	19

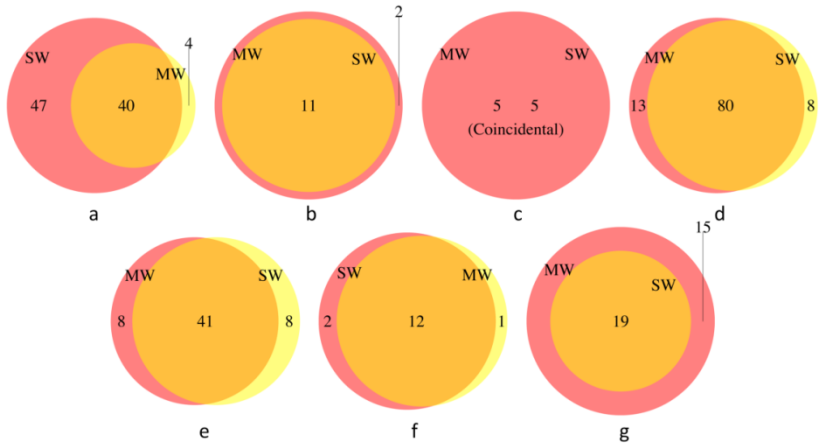

Figure 5 Overlap of the changes in protein abundance in common Biological Functions after 24 h exposure to a low concentration (100 ng/mL) of MWCNT or SWCNT. The numbers of proteins that are altered in response to low dose carbon nanotube exposure within defined biological functions are listed. The Venn diagrams show the number of proteins with shared identity altered in response to both MWCNT and SWCNT.

2.3.2.1 Upstream Regulators

Upstream regulator analysis can predict upstream molecules, including microRNA and transcription factors, which may be causing the observed protein expression changes. Table 1 lists the upstream regulators that were predicted to be activated or inhibited based on the activation z-score. Given the fold change of corresponding proteins, the state of the upstream regulators that control these proteins can be predicted. Only two upstream regulators, Fragile X mental retardation 1 (FMR1) and mitogen-activated protein kinase 1 (MAPK1), were shown to be activated with a z-score > 2, and the others were inhibited with z-score < −2. Many of these upstream regulators are cytokines or transcription

regulators. In general, the depression in upstream regulators indicates a stress response as well as an effect on the cellular defense mechanism which may make the airways more susceptible to attack by microorganisms. However, two of the upstream regulator pathways delineate control of intracellular processes that have direct applicability to the functional effects previously documented in the Calu-3 cells—namely a decrease in TEER or barrier function and a decrease in hormone-stimulated Cl^- secretion.

Adenosine receptor A2a (ADORA2A) is a receptor for adenosine. The activity of this receptor is mediated by a G protein that activates adenylyl cyclase. It has been shown that the inhibition of ADO-R *in vivo* prevented activation of CFTR and also resulted in airway surface liquid (ASL) height collapse and a failure to effect ASL height homeostasis [46]. This is in agreement with our observation of a decrease in epinephrine-stimulated Cl^- secretion via CFTR in Calu-3 cells after exposure to CNTs [24]. While a decrease in cellular transport phenomena may be a cellular response to stress, a decline in this specific pathway would enhance airway dehydration and have a deleterious effect on mucocillary clearance.

Coagulation factor II (F2) is also called prothrombin. It is proteolytically cleaved to form thrombin in the coagulation cascade, which ultimately results in the reduction of blood loss. In alveolar epithelial (A549) cells, thrombin induces activation of Rho and Rac that leads to MLC phosphorylation and formation of the peripheral actomyosin ring with peripheral accumulation of ZO-1/occludin complexes, thus enhanced barrier protection after acute lung injury [47]. A decrease in the pathway is consistent with the CNT-induced decrease in TEER that we have previously documented [24].

Table 1 Top upstream regulators mapped to common protein changes after exposure to low concentration (100 ng/mL) of SWCNT and MWCNT.

Upstream Regulator	Protein Names	Molecule Type	Predicted Activation	Activation z-score	*p*-value of overlap	Target molecules in dataset
FMR1	Fragile X Mental Retardation 1	Other	Activated	2.236	6.05E−05	CFL1, EEF2, PFKP, PPIA, UQCRFS1
MAPK1	Mitogen-activated Protein Kinase 1	Kinase	Activated	2.138	2.87E−02	EHD1, GRB7, LAP3, LGALS3BP, LMNA, MVP, STAT1, SUN2
NFE2L2	Nuclear Factor (Erythroid-derived 2)-like 2	Transcription Regulator	Inhibited	−3.884	3.00E−08	AKR7A2, ATP1A1, CTSD, DYNLL1, GNB2L1, HSP90AA1, LMNA, PDIA4, PDIA6, PSMA4, PSMB3, PSMC1, PSMD13, RARS, RPLP0, S100A13, STIP1, TXN, UGDH
TFEB	Transcription Factor EB	Transcription Regulator	Inhibited	−2.214	2.11E−05	CDH1, CTSD, HEXA, LAMP1, PSAP
ANGPT2	Angiopoietin 2	Growth Factor	Inhibited	−2.646	2.97E−04	HSP90AA1, HSPA1A, HSPA1B, HSPA2, HSPA4, NME1, P4HB, PDIA6
ADORA2A	Adenosine A2a Receptor	G-protein Coupled Receptor	Inhibited	−2.449	1.53E−03	ARF3, EEF2, P4HB, PPP2R1A, SPTBN1, USP5
INSR	Insulin Receptor	Kinase	Inhibited	−2.621	6.05E−03	ATP5A1, ATP5B, CFL1, CS, GRB7, HSD17B10, HSD17B4, MDH2, PDHB, SCP2
SYVN1	Synovial Apoptosis Inhibitor 1, Synoviolin	Transporter	Inhibited	−2.449	8.27E−03	ATP1A1, GNB2, ITGB1, LGALS3BP, MYOF, USP5
IFNG	Interferon, Gamma	Cytokine	Inhibited	−2.682	1.12E−02	AGRN, ATP1A1, CDH1, CTSC, CTSD, DHX9, ELAVL1, GNB2L1, HSD17B4, HSP90AA1, HSPA1A/HSPA1B, IL18, ITGB1, LGALS3BP, MX1, MYH9, PPIA, PSMA4, SERPINA1, STAT1, TYMP
CD40LG	CD40 Ligand	Cytokine	Inhibited	−2.449	2.44E−02	CTSC, HSP90AA1, HSPA1A, HSPA1B, MX1, NAP1L1, STAT1, TYMP, XRCC5, XRCC6

Table 1 Continued.

XBP1	X-box Binding Protein 1	Transcription Regulator	Inhibited	−2.2	2.47E−02	ARCN1, PDIA4, PDIA6, SERPINA1, TXN, XRCC6
F2	Coagulation Factor II (Thrombin)	Peptidase	Inhibited	−2.598	2.90E−02	CAD, HSP90AA1, ITGB1, LAMP1, MYH9, PDIA4, RNH1
IRF7	Interferon Regulatory Factor 7	Transcription Regulator	Inhibited	−2	3.97E−02	ATP5A1, MX1, STAT1, TMPO
STAT4	Signal Transducer and Activator of Transcription 4	Transcription Regulator	Inhibited	−2.425	4.51E−02	AHNAK, HEXB, HSPA1A, HSPA1B, MX1, SF3B1, STAT1

2.3.2.2 Canonical Pathways

Table 2 lists the pathways that had significant protein changes ($p < 0.01$) with a minimum of 2 proteins that represent at least 20% of the pathway. All of the 6 pathways were down-regulated. Four of the six identified canonical pathways are primarily involved in cell metabolism and energy production.

Glycogen degradation II and III represent glycogenolytic pathways that provide cellular energy. A decline in these pathways may reduce energy production and reflect an overall decrease in cell metabolism.

Bile acid biosynthesis neutral pathway is the major pathway of cholesterol catabolism in mammals. Methylglyoxal degradation III is a detoxification pathway of cell metabolism. The decrease in these processes may affect the metabolism of both lipid and carbohydrate. However, chronic exposure could ultimately compromise normal cellular metabolism and maintenance.

RAN is a member of the Ras family of small GTPases, and it plays a critical role in nucleo-cytoplasmic transport of macromolecules through the nuclear pore complex by

promoting assembly and disassembly reactions of transport receptors and cargo. Several proteins that were decreased in the RAN signaling pathway, IPO5, KPNB1, KPNA2, are importins and receptors that can bind with nuclear localization signal (NLS) and are involved in the import of proteins into the nucleus, while XPO1 mediates leucine-rich nuclear export signal (NES)-dependent protein transport [48]. The inhibition of this pathway may indicate a decrease of the nucleo-cytoplasmic transport and may affect cellular growth, proliferation and development.

Table 2 Top canonical pathways mapped to common protein changes after exposure to low concentration (100 ng/mL) of SWCNT and MWCNT.

Ingenuity Canonical Pathways	**−log(*p*-value)**	**Ratio**	**Molecules**	**Categories**	**Top Functions and Diseases**
Glycogen Degradation III	5.07	44.40%	GAA, PYGB, TYMP, MTAP	Glycogen Degradation	Developmental Disorder; Hereditary Disorder; Metabolic Disease
Glycogen Degradation II	3.63	37.50%	PYGB, TYMP, MTAP	Glycogen Degradation	Developmental Disorder; Hereditary Disorder; Metabolic Disease
RAN Signaling	4.07	26.70%	KPNB1, KPNA2, XPO1, IPO5	Cellular Growth, Proliferation and Development	Cell Signaling; DNA Replication, Recombination, and Repair; Nucleic Acid Metabolism
Bile Acid Biosynthesis, Neutral Pathway	2.15	25.00%	AKR1C1/AKR1C2, SCP2	Sterol Biosynthesis	Endocrine System Development and Function; Energy Production; Lipid Metabolism
Methylglyoxal Degradation III	2.04	22.20%	AKR7A2, AKR1C1/AKR1C2	Aldehyde Degradation	Endocrine System Development and Function; Energy Production; Lipid Metabolism
Telomere Extension by Telomerase	2.76	20.00%	XRCC6, HNRNPA2B1, XRCC5	Apoptosis; Cancer	Cellular Assembly and Organization; Cellular Function and Maintenance; DNA Replication, Recombination, and Repair

Telomeres are dynamic DNA-protein complexes that cap the ends of linear chromosomes, preventing detrimental chromosome rearrangements and defending against genomic instability and the associated risk of cancer. Telomerase, also called telomere terminal transferase, prevents telomere shortening and has high activity in lung cancer cell lines [49]. Two DNA repair proteins, XCRR5 and XCRR6, were decreased in the pathway of telomere extension by telomerase. This pathway is involved in the prevention of telomere degradation, chromosome clustering and apoptosis and inhibition may lead to the instability of chromosome and cell apoptosis. SWCNTs have been previously reported to inhibit telomerase activity through stabilization of i-motif structure eventually leading to telomere uncapping and displacement of telomere-binding proteins from the telomere, which triggers DNA damage [50].

2.3.2.3 Biological Functions

The top functions that were predicted with a significant activation z-score (Table 3), fell into categories of cell death and survival, cell-to-cell signaling and interaction, cellular assembly and organization, cellular growth and proliferation, cellular movement, infectious disease, molecular transport and protein synthesis. Among the functional changes, only cell death increased while the others decreased. The functional changes may indicate a protective response in which the cell decreases energy requiring activities and functions to protect itself [51].

In the function of cell death and cell survival, there were 78 and 34 proteins involved, respectively, and 31 of them were common to both SWCNT and MWCNT

exposures. Overall there was an increase of proteins associated with cell death and a decrease in proteins associated with cell survival. Interestingly, however, while the pathways were activated, our previous studies have indicated there was little actual cell death in 24 h [24,25]. This conclusion is based on the observation that while the TEER had a significant decline indicating a decrease in barrier function, the monolayer maintained a measureable TEER which would not be possible if the cells died and the junctional interactions were lost. So the decrease of these proteins may turn down the pathways that are essential for cell survival and basic metabolism and increase proteins associated with cell death. In future experiments, it will be interesting to determine if chronic (>24 h) exposure will actually cause a decrease in cellular viability.

Proliferation of cells was another similar function found to be decreased. As a human lung cancer cell line, Calu-3 cells have infinite division and proliferation potential. Despite the origin of this cell line, it does exhibit contact inhibition after a confluent monolayer is established. The maintenance of an electrically tight (high resistance) monolayer of cells indicates that within the 24 h time frame there was no increase in cell death. However, it should be noted that the proliferation is very low after the formation of an intact epithelium. The results indicate a decrease in proliferative capacity since the expression of proteins in this pathway was decreased by CNT exposure relative to controls. This may ultimately have deleterious effects on the ability of the cells to respond to noxious stimuli that cause cell death. Other factors involved in cell division are microtubule and actin filaments. Research by Holt et al. shows that cell proliferation is greatly reduced in SWCNT-treated cells with an increase in actin-related division

defects, due to actin bundling [52]. Thus these results are only predictive of what may happen under injury conditions.

In addition to cell proliferation, cell migration also plays an important role during *in vitro* wound repair of the respiratory epithelium [53]. Decreased expression of proteins known to be important for cell movement may lead to inhibition of epithelial wound repair. Actin filaments, usually in association with myosin, are responsible for many types of cellular movements and the breakdown of these processes may impair the motility of cells.

Synthesis of proteins, transport of proteins, and internalization of proteins were all decreased after exposure to CNTs, which means an inhibition of the protein metabolism. The decrease of eukaryotic translation initiation factor (EIF3B, EIF3I, EIF3L, EIF4A2) and eukaryotic translation elongation factor (EEF1A1, EEF2) indicates the inhibition of protein translation. Transmembrane emp24 domain-containing protein 10 (TMED10) and clathrin (CLTC) are involved in vesicular protein trafficking and the documented decrease of these proteins may slow down the intracellular trafficking of proteins and exocytosis and endocytosis of a variety of molecules.

In the function of cell-to-cell signaling and interactions, intercellular junction impairment is suggested by the decreased expression of five proteins, agrin(AGRN), capping protein muscle Z-line beta (CAPZB), E-cadherin (CDH1), desmoplakin (DSP), and junction plakoglobin (JUP). These proteins are components of tight junctions or adhesion junctions and barrier function. The change in junctional integrity is consistent with our previous results that exposure to 100 ng/mL of either CNT decreased the barrier function of the epithelial monolayer [24].

Recruitment of leukocytes including phagocytes, neutrophils, and granulocytes is important for an innate immune response, and this was also decreased. Research has shown that recruitment of leukocytes into the lungs in response to inhaled pathogens is initiated by epithelial signaling, the activation of toll-like receptors (TLRs), and the production of the chemokine interleukin-8 [54]. Airway recruitment of leukocytes in mice is dependent on alpha4-integrins and vascular cell adhesion molecule-1 [55]. In the CNT-treated cells, signaling proteins like interleukin 18 (IL18) and adhesion proteins like integrin alpha E (ITGAE) were decreased, which, *in vivo*, could compromise recruitment and trafficking of leukocytes into the bronchoalveolar lavage fluid.

The decrease in proteins associated with the response to viral infection also indicates an inhibition of anti-infection activity making the cells vulnerable to toxicants inhaled by respiration. This is also coincides with the decline of recruitment of leukocytes, and will further reduce the immune function of the cells.

The cellular components are present in a highly organized structure and there is an organized network that might act as a scaffold for cell [56]. A diminution of proteins involved in the functional organization of cytoplasm will result in changes in the assembly, arrangement of constituent parts, or disassembly of the cytoplasm. The interference of the organization of cytoplasm may lead to a disorder of the cellular contents and affect cell metabolism and function.

Table 3 Top functions mapped to common protein changes after exposure to low concentration (100 ng/mL) of SWCNT and MWCNT.

Category	Functions Annotation	*p*-Value	Predicted Activation		Molecules	#
			Activation	z-score		
Cell Death and Survival	Cell Death	9.03E−05	Increased	2.208	AGRN, ANXA1, ASAH1, ATP1A1, ATP5A1, BAG6, CCT6A, CDH1, CTNNA1, CTNNBL1, CTSD, DHX9, DSP, DYNLL1, EEF1A1, EHD1, EIF3B, EIF3I, ELAVL1, EZR, GNB2, GNB2L1, GRB7, GSN, HDGF, HEXB, HSD17B10, HSP90AA1, HSPA1A, HSPA1B, HSPA2, HSPA4, IL18, ITGB1, JUP, KPNA2, LAMP1, LGALS3BP, LMNA, MCM10, MVP, MX1, MYH9, NDUFS3, NME1, NOD1, P4HB, PARK7, PCBP2, PPIA, PPP1R11, PPP2R1A, PSAP, PSMC1, PSMD9, PTGES3, PYCARD, RPLP0, RPS3A, SCP2, SERPINA1, SND1, SPR, SPTBN1, STAT1, STIP1, SUN2, TARDBP, TMED10, TPT1, TRPM7, TXN, TYMP, UQCRFS1, XPO1, XRCC5, XRCC6, YARS, YWHAQ	78
	Cell Survival	5.14E−03	Decreased	−3.955	AGRN, ASAH1, CDH1, CHD4, DHX9, EEF2, ELAVL1, EZR, GNB2L1, GRB7, HDGF, HSD17B10, HSPA1A, HSPA1B, HSPA4, IL18, ITGB1, JUP, LMNA, MVP, MX1, NME1, P4HB, PARK7, PPP1R11, PPP2R1A, PSMA4, PYCARD, SND1, STAT1, TARDBP, TXN, TYMP, XPO1, XRCC5	34
Cell-to-cell Signaling and Interaction	Quantity of Intercellular Junctions	2.91E−04	Decreased	−2.186	AGRN, CAPZB, CDH1, DSP, JUP	5
	Recruitment of Leukocytes	5.22E−03	Decreased	−2.156	ANXA1, CTSC, FLOT1, GSN, HSPA1A/HSPA1B, IL18, ITGAE, NOD1, PYCARD, TPT1, TXN	11
Cellular Assembly and Organization	Organization of Cytoplasm	6.56E−03	Decreased	−2.522	ADD1, AGRN, ARPC2, CAPZB, CDH1, CFL1, CLTC, DSP, DYNLL1, EEF1A1, EZR, FLOT1, GAA, GSN, HDGF, HEXA, HEXB, HSP90AA1, ITGB1, JUP, KPNB1, MYH9, NME1, PFN2, PLS3, RRBP1, SCP2, SEPT9, SLC9A3R1, SPTBN1, STIP1, SUN2, TMED10, XPO1	34

Table 3 Continued.

Cellular Growth and Proliferation	Proliferation of Cells	8.39E−05	Decreased	−4.147	AGRN, AHNAK, AKR1C1, AKR1C2, ANXA1, ARF1, ASAH1, ASH2L, ATP5A1, ATP5B, C19orf10, CDH1, CFL1, CHD4, CLTC, CTNNA1, CTSC, CTSD, DSP, EEF1A1, EIF3B, EIF3I, ELAVL1, EZR, FLOT1, GALNT2, GNB2L1, GRB7, GSN, HDGF, HEXB, HNRNPA2B1, HNRNPAB, HNRNPD, HNRNPR, HNRNPU, HSPA1A, HSPA1B, IL18, ITGB1, JUP, KPNA2, LMNA, MAPRE2, MCM10, MTAP, MVP, MX1, MYH14, MYH9, MYOF, NAP1L1, NDUFS3, NME1, PARK7, PFKP, PFN2, PPIA, PPL, PPP2R1A, PSAP, PSMC1, PSMC2, PSMD2, PYCARD, RAB1A, RNH1, RPS3A, S100A13, SEPT9, SERPINA1, SLC9A3R1, SND1, SPTBN1, STAT1, TARDBP, TMPO, TPT1, TRPM7, TXN, USP5, XRCC5, XRCC6, YWHAQ	82
Cellular Movement	Cell Movement	1.37E−02	Decreased	−2.804	ADD1, ANXA1, ARF1, CDH1, CFL1, CTNNA1, CTSC, EHD1, EZR, FLOT1, GALNT2, GNB2, GNB2L1, GRB7, GSN, HARS, HDGF, HNRNPA2B1, HSP90AA1, HSPA1A, HSPA1B, IL18, ITGAE, ITGB1, JUP, KPNA2, LMNA, MTAP, MX1, MYH9, NME1, NOD1, PARK7, PPIA, PYCARD, RNH1, SEPT9, SERPINA1, SLC9A3R1, STAT1, TPT1, TXN, TYMP, UGDH, YARS	44
Infectious Disease	Viral Infection	4.96E−03	Decreased	−4.338	ARCN1, ARF1, ATP5B, BAG6, CAD, CLTC, DHX9, EEF1A1, EIF3I, G3BP1, HNRNPH1, HNRNPU, HSP90AA1, IL18, ITGB1, KPNB1, LMNA, MVP, MX1, MYOF, PCBP2, PDIA6, PFKL, PPIA, PSMD2, PTGES3, PYCARD, RNH1, RPS10, SERPINA1, SERPINB6, SF3B1, SFPQ, SLC9A3R1, SPTBN1, STAT1, STIP1, TMPO, TPT1, TXN, UQCRFS1, XPO1	42
Molecular Transport	Internalization of Protein	5.38E−04	Decreased	−2	CFL1, CLTC, JUP, KPNA2, KPNB1, SPTBN1, XPO1	7
	Transport of Protein	2.51E−03	Decreased	−2	ARF1, ARF3, CFL1, EHD1, JUP, KPNA2, KPNB1, MYH9, RAB1A, SPTBN1, TMED10, XPO1	12
Protein Synthesis	Synthesis of Protein	2.06E−05	Decreased	−2.031	DHX9, EEF1A1, EEF2, EIF3B, EIF3I, EIF3L, EIF4A2, ELAVL1, GNB2L1, GRB7, GSN, IGF2BP2, IL18, ITGB1, KRT7, PARK7, RPS3A, RRBP1, STIP1	19

2.3.3 Protein interaction Networks

The STRING database was used to predict protein interaction networks of functionally related proteins and to provide an enhanced definition of the functions described in the section above by revealing the individual interactions of the proteins that are altered in response to CNT exposure. This analysis provides uniquely comprehensive coverage of both experimental and predicted interaction information and the software gives a relative confidence score [39]. We focused on protein interactions with a medium confidence score >0.4. The interactions are represented by knots connected with edges (lines). In Figure 6, thicker edges represent stronger associations. For each protein-protein interaction network, the majority of the knots were linked with each other, while some of the altered proteins were isolated without partners. Although most proteins interact with only one or two others, a few are "hub" proteins capable of physically interacting with many partners. In this sense, the networks do not appear to be random, meaning that each protein would have a similar number of binding partners but are, rather, considered scale-free [57]. Scale-free networks have certain important characteristics, such as unequal binding interactions and hubs that have an unusual number of binding partners. This type of network is common in biological systems and leads to a certain redundancy within the network but, at the same time, also creates system vulnerability if a hub protein expression/activity is altered.

Within the various networks, Cadherin 1 (CDH1), signal transducer and activator of transcription 1 (STAT1), junction plakoglobin (JUP), ezrin (EZR) apoptosis-associated speck-like protein containing a CARD (PYCARD), are connected with many partners, which suggest they are important hub proteins and may be more important biologically

than less connected nodes [58]. The modulation of their expression will, therefore, have more effect on the cell function. For instance, EZR, an intermediate between the plasma membrane and the actin cytoskeleton proteins, is essential for epithelial cell integrity and can also regulate the structure and the function of specific domains of the plasma membrane. It plays a key role in cell surface structure adhesion, migration, and organization [59]. PYCARD is composed of two protein-protein interaction domains, PYD and CARD, that mediate assembly of large signaling complexes in the inflammatory and apoptotic signaling pathways via the activation of caspase-1 [60].

Furthermore, it was found that some hub proteins appeared in several networks. JUP appeared in 8 of the total 11 functions, while IL18 and integrin beta-1 (ITGB1) were involved in 7 functions. Exportin-1 (XPO1), thioredoxin (TXN), spectrin beta chain non-erythrocytic 1 (SPTBN1), PYCARD, gelsolin (GSN), and cadherin 1 (CDH1) took part in half of the main cellular functions that were altered in response to CNT exposure.

Despite the interactions, CNT-altered proteins linked to each individual function are located in different parts of the cell and involved in different cell activities. For example, proteins involved in cell skeleton and membrane, nuclear transportation, transcription, cell junction, were all connected with each other. In Figure 6 of interaction of proteins within functional network of “Cell Death”, proteins that are component of adherens junctions can interact with proteins that are component of ribonucleoprotein complex. Therefore, each function is integrated throughout the cell forming a whole cell adaptive response.

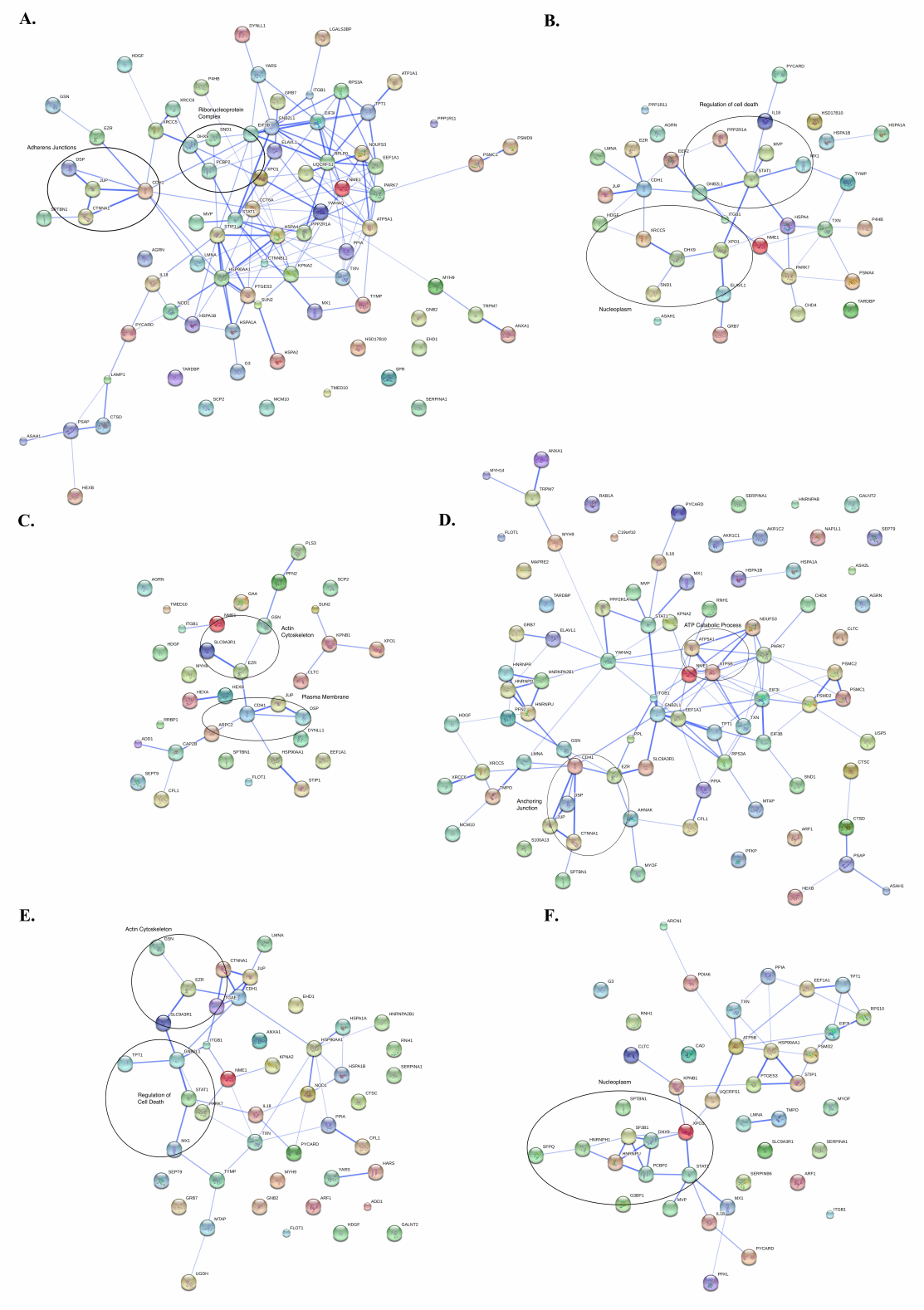
A.
Ribonucleoprotein Complex
Adherens Junctions
B.
Regulation of cell death
Nucleoplasm
C.
Actin Cytoskeleton
Plasma Membrane
D.
ATP Catabolic Process
Anchoring Junction
E.
Actin Cytoskeleton
Regulation of Cell Death
F.
Nucleoplasm

Figure 6

Figure 6 Identity and interaction of proteins within functional network that are altered by 24 h carbon nanotube exposure. STRING database was used to illustrate the interactions of the proteins that were altered by exposure to a low dose of both SWCNT and MWCNT. The strength of the interactions is indicated by the thickness of the connecting lines. Proteins that have no connecting lines have been identified as altered by both SWCNT and MWCNT exposure but are not part of a network that connects them to any of the other altered proteins. (A) Proteins within functional network of "Cell Death". Proteins in the left circle are component of adherens junctions, and proteins in the right circle are component of ribonucleoprotein complex. Hub proteins in the network: RPLP0, ribosomal protein large P0; RPS3A, ribosomal protein S3A; EEF1A1, eukaryotic translation elongation factor 1 alpha-like 7; TPT1, tumor protein translationally-controlled 1; HSP90AA1, heat shock protein 90 kDa alpha (cytosolic) class A member 1; STAT1, signal transducer and activator of transcription 1, 91 kDa; STIP1, stress-induced-phosphoprotein 1; CDH1, cadherin 1 type 1 E-cadherin (epithelial); JUP, junction plakoglobin; (B) Proteins within functional network of "Cell Survival". Proteins in the upper circle are involved in the regulation of cell death, and proteins in the lower circle are located on the nucleoplasm. Hub proteins in the network: CDH1; STAT1; (C) Proteins within functional network of "Organization of Cytoplasm". Proteins in the upper circle are component of actin cytoskeleton, and proteins in the lower circle are located on plasma membrane. Hub proteins in the network: CDH1; (D) Proteins within functional network of "Proliferation of Cells". Proteins in the left circle are component of anchoring junctions, and proteins in the right circle are involved in the ATP catabolic process. Hub proteins in the network: JUP; EZR, ezrin; CDH1; LMNA, lamin A/C; HNRNPR, heterogeneous nuclear ribonucleoprotein R; GNB2L1, guanine nucleotide binding protein (G protein), beta polypeptide 2-like 1; TPT1; STAT1; (E) Proteins within functional network of "Cell Movement". Proteins in the upper circle are component of actin cytoskeleton, and proteins in the lower circle are involved in the regulation of cell death. Hub proteins in the network: HSP90AA1; CDH1; GNB2L1; (F) Proteins within functional network of "Viral Infection". Proteins in the circle are located on the nucleoplasm. Hub proteins in the network: STAT1; HNRNPU, heterogeneous nuclear ribonucleoprotein U (scaffold attachment factor A); TPT1.

CHAPTER 3. EFFECTS OF CARBON NANOTUBES ON MODEL LIPID BILAYERS

3.1 CNT's effect on lipid bilayer

The cell membrane separates the intracellular components from the outside environment. It is selectively permeable to ions and organic molecules and controls the movement of substances in and out of cells. It is a strong barrier to protect the cell from its surroundings while allowing nutrient and waste exchange.

As shown by experimental evidence and SEM images, high aspect ratio carbon nanotubes can cross the plasma membrane and get into cells. One description of this kind of cell entry is considered to be energy-dependent and occurs by tip recognition and rotation at the tube–bilayer interface [61]. The cell membrane is composed of lipid bilayer and proteins including receptors, ion channels and signaling proteins. Nanoparticles can alter the physical properties of lipid membranes and therefore could influence lipid and protein functions [62]. Our previous studies showed that CNT exposure over a wide range of concentrations could cause the decrease of TEER in airway and renal epithelial cells and secretory Cl^- flux that is stimulated in response to epinephrine in the airway cells [24,25,63].

Phospholipids make up 25% to 80% by weight of cell membranes, and each has a hydrophilic head and two hydrophobic tails. When dissolved in water or polar solvent, they can form a bilayer spontaneously so that the hydrophobic tails are isolated from the

surrounding polar fluid and hydrophilic heads are exposed. These artificial bilayers are similar to natural membranes and have been used as a model to study the properties and functions of cell membrane [64]. By molecular dynamic simulation, short SWCNTs are found to reduce the mobility of lipid molecules in a DOPC bilayer and to perturb the structure of interfacial water, which suggests that the perturbations in the lipid structure of nanotubes could lead to enhanced penetration of molecular compounds across the membrane [65]. More experimental research needs to be done to clarify how CNTs interact with the lipid membrane and the proteins that are suspended in them.

In our study, we built model lipid membranes with a planar bilayer workstation, and investigated the interaction of short purified MWCNT with the lipid membrane and ion channels. The electrophysiology measurement of ion movement across lipid bilayers induced by CNTs can help to understand the interaction of lipid bilayer with CNTs.

3.2 Methods

3.2.1 Bilayer lipid membrane synthesis

The lipid, 1, 2-diphytanoyl-sn-glycero-3-phosphocholine (DPhPC) was purchased from Avanti Polar Lipids (Alabaster, AL). Bilayer lipid membranes were formed using a Planar Bilayer Workstation (Black Lipid Membranes, BLM), Warner Instruments, coupled with a stereo microscope. The workstation was comprised of a Faraday cage with vibration isolation table, Model FC-1, which houses the BLM chamber and the electrical circuitry.

To synthesize a membrane, 2400 µl of 1 M potassium chloride (KCl) buffer was added to each well of the chamber and then a pair of 3 ml syringes was connected to the

chamber wells. These were used to manipulate the buffer volume in each well. The wells were separated by partition containing a small hole in a Teflon tape. The buffer was lowered below the hole in the Teflon tape and the stereo microscope was used to ensure that the level was low enough. Using a 10 µl capillary tube, 10 µl of the DPhPC dissolved in pentane (2 mg/mL) was added to the surface of the buffer in each well. Approximately 0.5 µl of hexadecane was then placed over the hole using a pipet tip for delivery. This was done while viewing the tip through the microscope. Five to seven min after adding the lipid, the buffer was raised above the hole by injecting it with the syringes to form a membrane. The lipid bilayer membrane usually has a diameter of less than 70 µm and thickness of 5 nm.

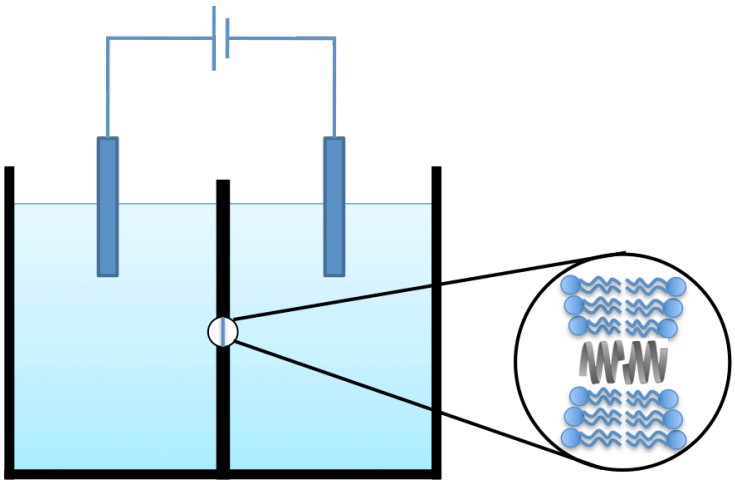

Figure 7 Image showing set-up of the apparatus for the synthesis of the lipid membrane.

Figure 7 shows the basic set-up for the apparatus after the buffer had been raised above the hole. The formation of the membrane within the Teflon tape was detected by current, conductance, and voltage readings on the electrical equipment. The oscilloscope was used to assess the presence and stability of a membrane. The Bilayer clamp

Amplifier, model BC-535; and the Low pass Bessel Filter 8 pole (Hamden, CT) were used to monitor the membrane stability and channel activity.

When a stable membrane was formed, the capacitance was noted to be around 100 pF. The baseline current across the membrane ranged from 0 to 2 pA and the voltage was set to zero. The membrane was allowed to stabilize for 10 min, and then a voltage of 100 mV was applied to ensure that there was no residue of any channel-forming agent, for instance gramicidin A (gA), left in the chamber. Without any gA, there should be no significant changes in the current or capacitance of the membrane and the formed membrane would show as a flat line on the Clampfit Electrophysiology Data Acquisition and Analysis Software. The electrical circuitry along with the Clampfit software generated graphs depicting the status of the membrane activity.

3.2.2 MWCNT on bilayer lipid membrane protocol

The purified MWCNTs (#900-1270) were purchased from SES Research (Houston, TX, USA) and had a reported outer diameter of 40-60 nm with the length ranging from 1-2 μm. The purity was reported to be >95%CNT with amorphous carbon <2% wt and ash content <2% wt. The MWCNTs were prepared as described in the CNT preparation for cell culture in section 2.2.2. After sonication, the samples were autoclaved and diluted to the final concentrations of nanoparticles in the serum-free cell culture media. For the control samples, FBS without nanoparticles was treated in an identical manner. There was a final concentration of 2% FBS in cell culture media.

1 μl of 10^{-15} M of the model ion channel protein, gA, was added to the buffer in each well. The channels were allowed to form and propagate for 30 min, after which MWCNT

in 2% FBS cell culture media was added to the wells with the final concentration of 2 μg/ml MWCNT and 0.04% FBS. The effect on the membrane was measured for 90 min and the resultant channel activity was assessed compared to the control with only 2% FBS media added.

To examine the effect of MWCNT in FBS on gA channels, MWCNT was prepared in FBS as described in section 2.2.2. After sonication, MWCNT in FBS was added directly to the wells on both sides of the lipid bilayer with a final concentration of 2 μg/ml MWCNT and 0.04% FBS. To examine the effect of MWCNT in 1M KCl on gA channels, MWCNT was prepared in 1M KCl. After sonication, MWCNT in 1M KCl was added to the wells with a final concentration of 2 μg/ml MWCNT. To examine the effect of MWCNT in DPhPC on gA channels, MWCNT was mixed with 2mg/ml DPhPC in pentane and was added to both sides of the membrane with a final concentration of 2 μg/ml after sonication.

3.2.3 Data analysis

Clampfit module of pClamp 10.1 software was used for the analysis of the Bilayer Lipid Membrane data. Measurements of ion channel duration and peak currents were carried out using the statistics module of Clampfit. The parameters measured were: the channel amplitude, which was the current reached at the peak of the open channel, the probability of an ion channel being open, and life-time (dwell time) of an opening channel. Statistical analyses of data were carried out using Sigmaplot 12.5 and Microsoft Excel software packages.

3.2.4 Analysis of particle size by Dynamic Light Scattering

1M KCl solutions containing MWCNT with a gradient of concentrations from 5mg/ml to 5ng/ml were analyzed using a Nano Zetasizer ZS90 (Malvern Instruments, Worcestershire, UK). In this technique, particle size is the diameter of the sphere that diffuses at the same speed as the particle being measured. The Zetasizer system uses dynamic light scattering (DLS) to measure the Brownian motion of the particles in a sample.

Since smaller particles move rapidly in a liquid than larger particles, the position of two images of the sample separated by a short interval of time is used to determine the displacement of the particle and therefore its relative size. A minimal displacement with similar particle positions indicates that the particles in the sample are large whereas larger displacements with different particle positions indicate that the particles in the sample are small. Using this principle and the relationship between diffusion speed and size, the relative sizes can be determined.

3.3 Results and Discussion

3.3.1 MWCNTs on bilayer lipid membrane

The lipid, 1, 2-diphytanoyl-sn-glycero-3-phosphocholine (DPhPC) has often been used in the study of protein-lipid interaction and membrane channel activity because of its high mechanical and chemical stability as well as high electrical resistances. With one hydrophilic head and two hydrophobic tails, DPhPC can form a neutral charged lipid bilayer similar to the plasma membrane. The membrane was formed using a Planar Bilayer Workstation (Black Lipid Membrane) from Warner Instruments following the

protocol described in section 3.2.1 and 3.2.2. With this instrument, the ionic currents were monitored when a voltage was applied across the bilayer lipid membrane. Once the membrane was stabilized, there was a characteristic flat baseline, which remained at the 0 pA level even when a voltage of up to 300 mV was applied. (The membrane would break at a voltage of 400 mV, which is used to check membrane integrity.)

The linear peptide gramicidin A (gA) forms prototypical ion channels specific for monovalent cations and has been extensively used as a model membrane protein and ion channel to study the organization, dynamics and function of membrane-spanning channels [66]. As shown in Figure 8, the gA channel is formed when a pair of gA monomers residing in opposite monolayers bind at the membrane center with N-terminus forming ion-conductive dimers, and the channel is closed when the dimers dissociate within the membrane [67]. When a voltage is applied across the membrane, the channels allow monovalent cations to pass through and generate a characteristic ionic current that can be measured.

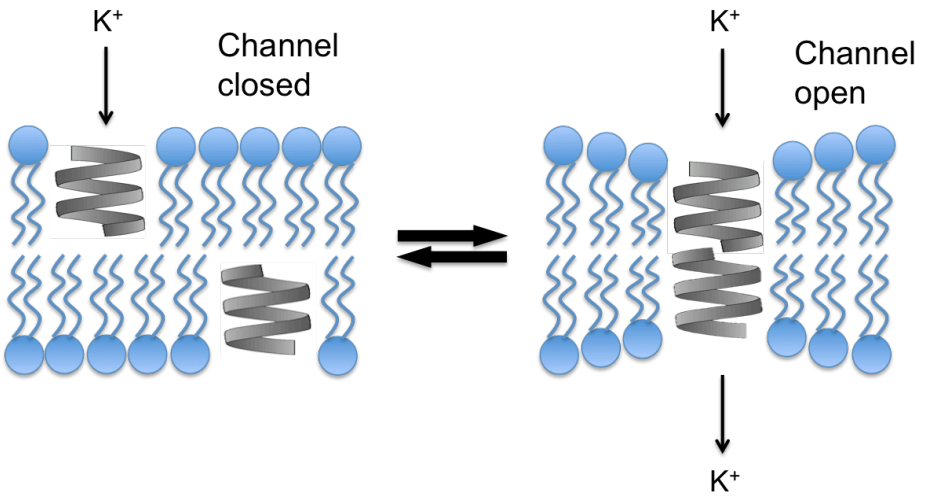

Figure 8 Selectivity and states of open and closed of gA channels.

In the presence of very small amounts of gramicidin, the membrane current under fixed applied voltage fluctuates in a well-defined step-like manner that is characteristic of channel openings. A record for the membrane formed by DPhPC in 1 M KCl with 1 µl of 10^{-15} M gA is shown in Figure 9. For the period of 270-295 s, the plot showed a flat baseline, which indicated an intact lipid bilayer. Lipid membranes are impermeable to ions without the presence of proteins or peptides that facilitate ion movement across the cell. At time = 295 s, there was an increase in current with the amplitude of 2.25 pA, which represented a single open channel (level-1 channel) in the membrane. At time = 302 s, there was a second increase in current of the same amplitude and was followed by a steady current, which displayed the duration of time two channels remained open (level-2 channel), ~1 s. The decrease in current at time =303 s and 315 s indicated the sequential closing of the two channels and the current returned to baseline.

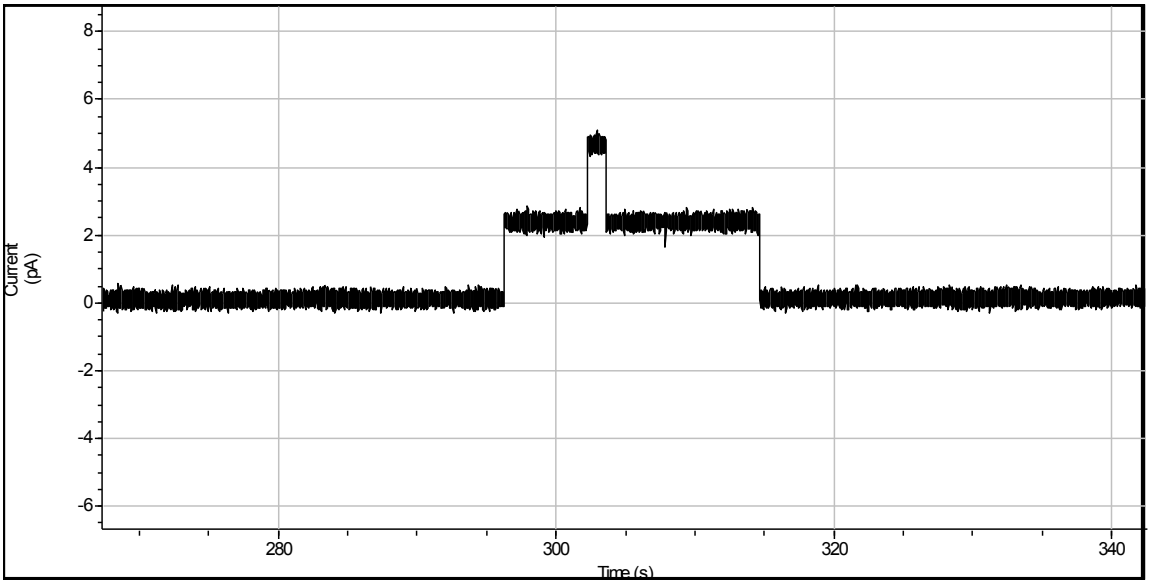

Figure 9 A representative recording of current as a function of time with DPhPC lipid at 100 mV. 1 µl of 10-15 M gA was added to the membrane at time = 0 s. The current baseline was 0 pA, the level-1 channel was 2.25 pA, and the level-2 channel was 4.51 pA.

The opening and closing of the gramicidin channel fit a Markov process, which means the present state of the system, its future and past are independent. And also the state of one gramicidin channel is independent from the others. Based on protein dynamics, the lifetimes (durations) of ion channels are considered to follow exponential or multiexponential distributions [68], as represented by the exponential decay in the frequency towards long durations. The probability of a certain number of channels open at any given time can be given by Poisson Distribution [69], which indicates that there are many gramicidin molecules available to form channels, while only a small proportion of them do so in any given interval. These statistical models are used to analyze and estimate the lifetime and open probability of the ion channels.

3.3.1.1 MWCNT in 2% FBS media on gA

When the membrane and gA channels were stable, MWCNT in 2% FBS media was added into both sides of the membrane for a final concentration of 2 μg/ml MWCNT and 0.04 % FBS. As shown in Figure 10, there was no detected single channel and current kept increasing until the membrane broke. The situation was similar for the control with 2% FBS media added.

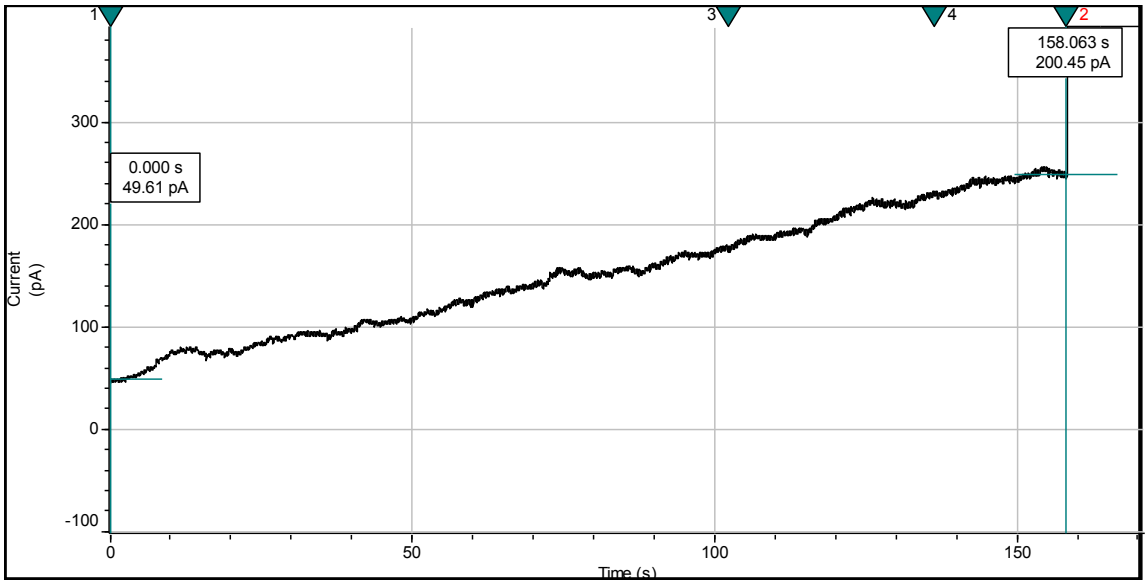

Figure 10 A recording of current as a function of time with DPhPC lipid and 1 µl of 10-15 M gA at 100 mV. MWCNT in 2% FBS media was added to the membrane at time = 0 s with the final concentration of 2 µg/ml MWCNT and 0.04 %FBS.

Comparison of the slope of current rise is shown in Figure 11. The slope of current rise according to time was around 1.25 pA per second. Although the values appeared to be different, Students' t-test showed that there is no significant difference between the control and MWCNT treated ones with the p-value of 0.606.

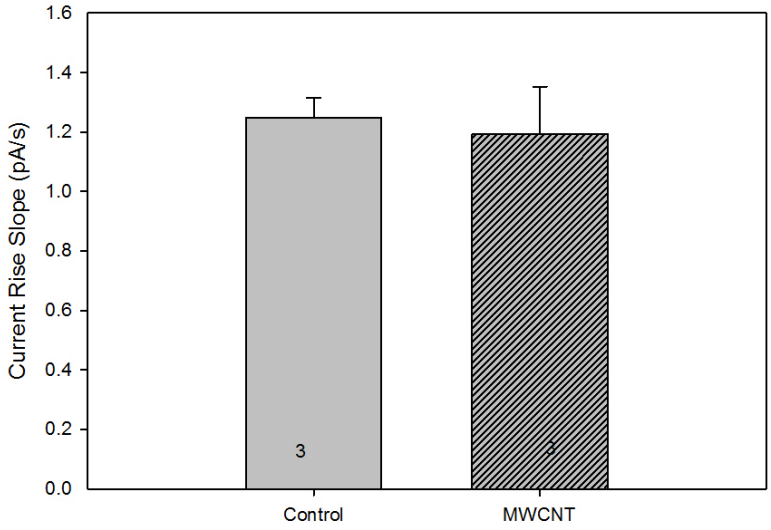

Figure 11 Comparison of the slope of current rise according to time in pA/s between the MWCNT in 2% FBS media treated group and 2% FBS media treated group as control. Student's T-test P-value = 0.606, n = 3 and 3 respectively.

There may be a few factors involved in this phenomenon. With the complexity of the components, the 2% FBS media may cause leakage of the lipid membrane. When DPhPC formed a bilayer membrane, it was stable and impermeable and in a dynamic balance. Under this circumstance, the movement of ions through the gA channels is well characterized by the statistics model. The presence of 2% FBS media may have some effect on the lipid molecules and cause disorder in the lipid bilayer system. Under the electric driving force, ions may move according to charge and break the balance, which was represented by the increase of the current and break of the membrane. During the increase of the current, several channels may also be involved. Usually, only small proportion of the large amount of gA monomers inserted into the bilayer can form open channels. Interaction of FBS and other components in the media with gA channels could increase the number of open channels and keep them open continuously. Besides,

proteins and other components in the media including penicillin and Glutamax also can insert into membrane and form ephemeral channels that ions can pass. On this background effect, the addition of MWCNT did not result in further slope change, as shown in Figure 11.

3.3.1.2 2% FBS media on membrane

To test the effect of 2% FBS media on membrane, the 2% FBS media was added directly onto the well-formed membrane in a gradation of volumes without presence of gA. When the media was added, some "peaks" appeared on the positive direction of the baseline as shown in the first 20 s of Figure 12, which indicated short current occurred at these points. The bandwidth limitations of the recording apparatus can cause events to be missed or their timecourse to be distorted, especially for short openings and short closings. More experiments showed that with the increase of the media volume, the fluctuation of the flat current baseline became stronger and when 100 μl of 2% FBS media was added (final concentration of 0.08% FBS), there was an increase of the current at time = 34 s with the amplitude of around 4 pA and at time = 182 s, the membrane had a sudden break. No single channel was detected during the whole process.

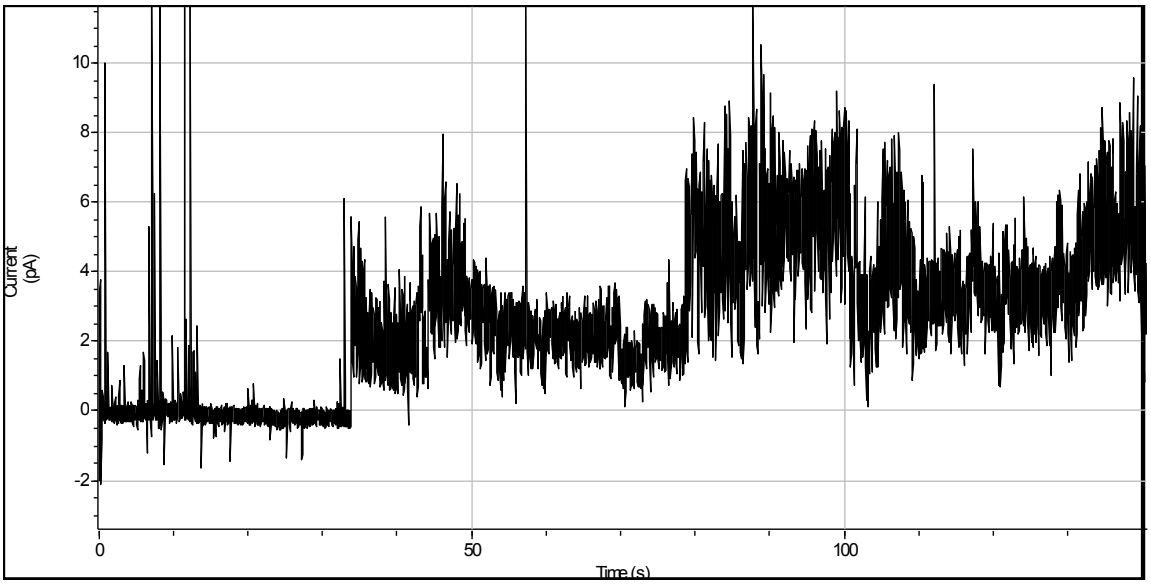

Figure 12 A recording of current as a function of time with DPhPC lipid at 100 mV. 2% FBS media was added to the membrane at time = 0 s with the final concentration of 0.08% FBS.

From the data shown in Figures 10-12, it was concluded that components in 2% FBS media have effects on the membrane with or without the presence of gA. Even through the media is essential for CNT preparation when used in cell culture experiments, it is not an ideal solution for the study using a bilayer lipid model because of its molecular complexity.

3.3.1.3 MWCNT in FBS on gA

To eliminate the effect of the media on membrane, the CNT was prepared in FBS without additional serum free media and was added directly onto the membrane. As shown in Figure 13, when 1 µl MWCNT in FBS was added with a final concentration of 2 µg/ml MWCNT and 0.04 %FBS, the well-defined step-like channels formed by 1 µl 10^{-15} M of gA grew wider but still in step-like shape. A closer look at these opening

channels indicated there are many short closings during the long opening of channels. The amplitude of the single open channel also decreased from around 2.25 pA to around 1.61 pA, which indicated a decrease of the conductance of the ion channel.

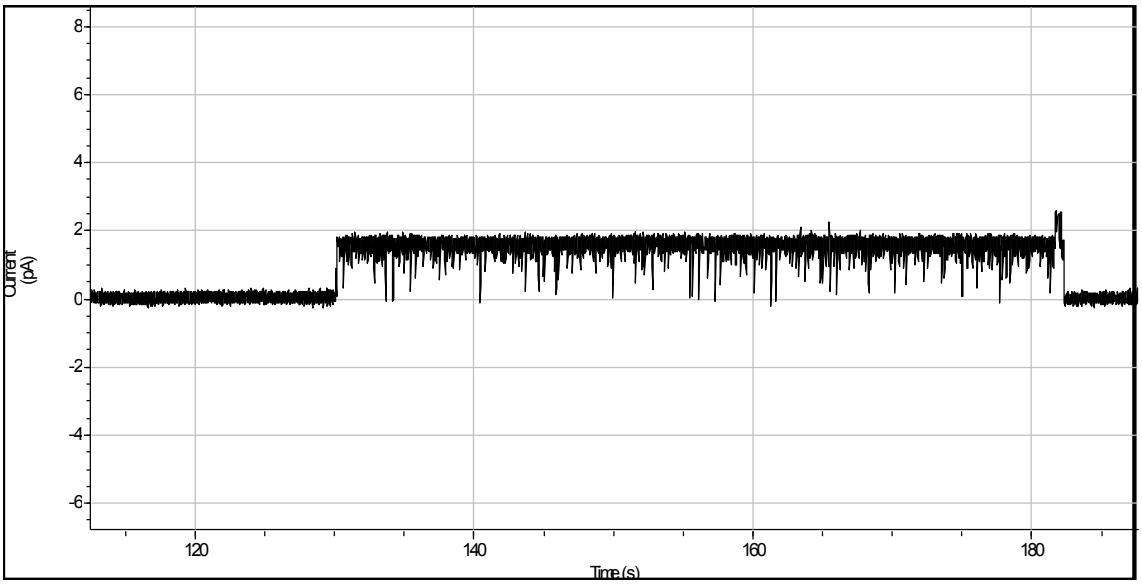

Figure 13 A recording of current as a function of time with DPhPC lipid and 1 µl of 10-15 M gA at 100 mV. MWCNT in FBS was added to the membrane at time = 0 s with the final concentration of 2 µg/ml MWCNT and 0.04 %FBS. The current baseline was 0 pA, and the level-1 channel was 1.61 pA

By convention, current is said to flow in the direction that positive charges would move. As described by Ohm's Law (I=gV), where the current (I, units Amperes) is proportional to the applied voltage (V, units Volts). The proportionality constant g is the conductance (units Siemens). A comparison of conductance of single channel (level-1) gA channels in the presence and absence of the MWCNT in FBS and FBS alone is shown in Figure 14. The average conductance of well-formed gA channel was 22.50 pS, while the presence of 2 µg/ml MWCNT in 0.04 % FBS caused a decreased conductance to an average of 16.09 pS. Interestingly, the FBS only treated channels had the lowest

conductance of around 12.88 pS. One-way ANOVA resulted with p-value < 0.01, which indicated a significant difference between these groups.

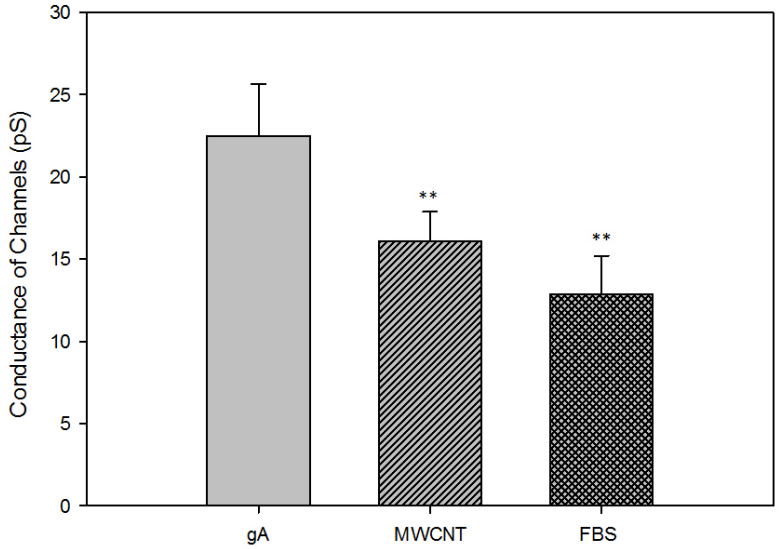

Figure 14 Comparison of the conductance in pS of well-formed gA channels and the MWCNT in FBS treated and FBS treated group. One-way ANOVA P-value < 0.01.

Under the conditions shown in Figure 13, the baseline was unaltered while all the disturbances occurred during channel openings, which indicated the effect should be on the gA channels instead of the DPhPC lipid bilayer. These short closing during the long opening of channels could be resulted from the transient blocking of the opening gA channels by FBS or MWCNT or quick dissociation and reassembly of the gA dimers.

A comparison of the conductance of gA channels under the three conditions indicated the blocking of channels should be most likely ascribed to FBS, which can explain the further decrease of channel conductance caused by only FBS. Research had shown that proteins in FBS could coat the surface of MWCNT when cultured together [42], which could cause an actual decrease of concentration of the FBS in solution. The

decrease of amount of FBS in the MWCNT-FBS group may reduce the effect of FBS on gA channels compared with the FBS group, as shown in Figure 14.

FBS is the blood fraction remaining after depletion of cells, fibrin and clotting factors in blood that comes from bovine fetus [70]. It is widely used in cell culture media because of it has a large number of nutritional and macromolecular factors essential for cell growth. It also contains small molecules including amino acids, sugars, lipids, hormones and ions like K^+, Na^+, Ca^+, Cl^-. The complexity of the components of FBS may have an effect on the gA channels, which remains unclarfied and will require more studies. However, it is clear that under these experimental conditions, it would be difficult to discern the effects of MWCNT on gA in artificial mambranes.

3.3.1.4 MWCNT in 1M KCl on gA

To avoid bringing in any components that may have effect on the membrane, the MWCNTs were prepared in 1M KCl alone. 1 µl of MWCNT in 1M KCl was added directly onto the membrane with the MWCNT final concentration of 2 µg/ml. Without the presence of FBS, the gA channel showd less electrical “noise” of rapid open and closing and the conductance of the single open channel was around 20.96 pS (Figure 15). Further analysis of the open probability and lifetime of the channels was done by Clampfit 10.1.

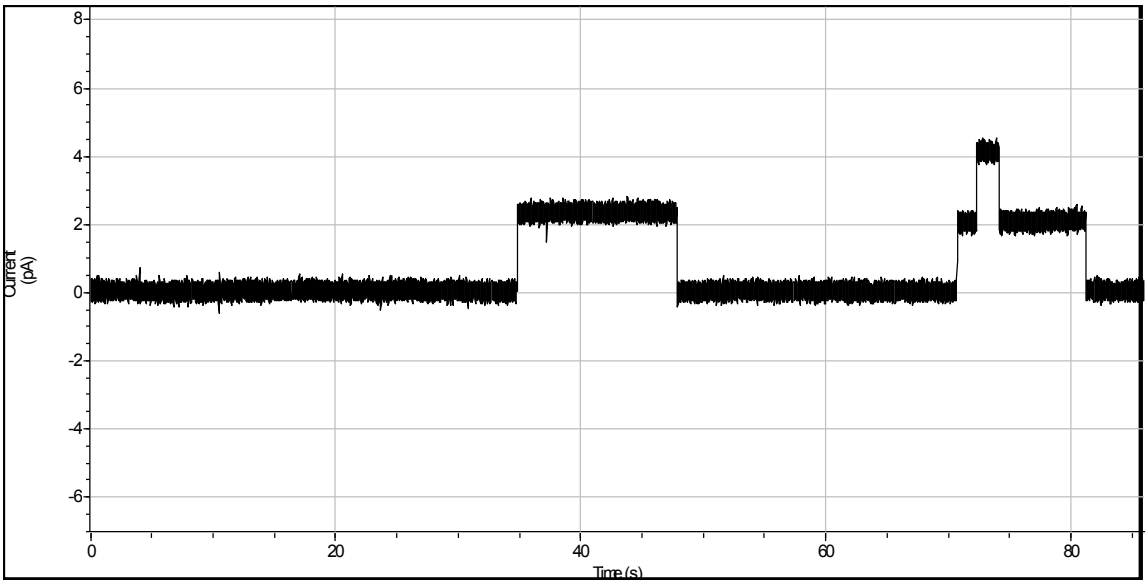

Figure 15 A recording of current as a function of time with DPhPC lipid at 100 mV. MWCNT in 1M KCl was added to the membrane at time = 0 s with the final concentration of 2 µg/ml. The current baseline was 0 pA, the level-1 channel was 2.10 pA and lever-2 channel was 4.21 pA

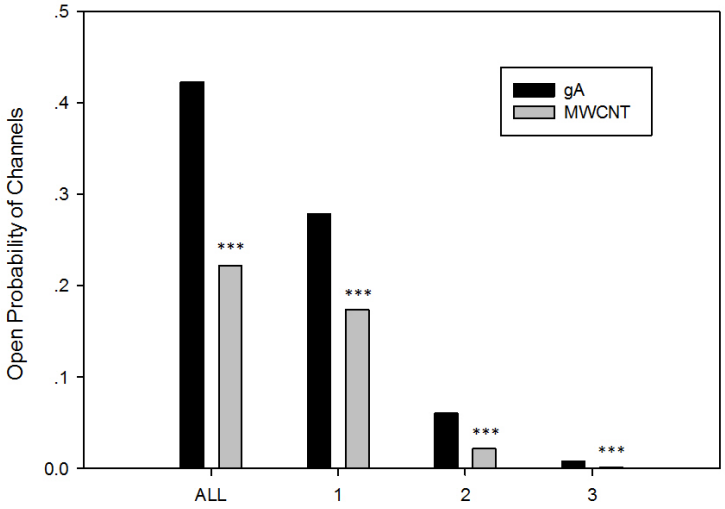

Figure 16 Comparison of the open probability of the channels in different levels between gA channels in the presence and absence of 2 mg/ml MWCNT. Three replications of experiments with hundreds of ion channels presence, P-value < 0.001.

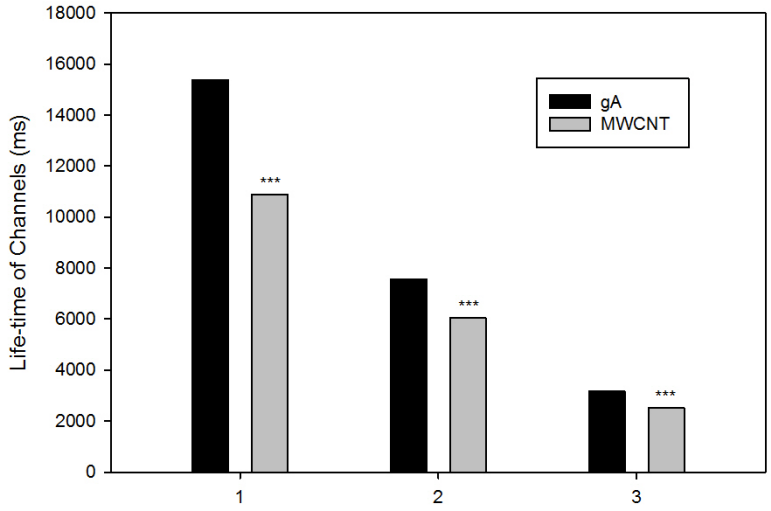

Figure 17 Comparison of life-time of the channels in millisecond (ms) of different levels between well-formed gA channels in the presence and absence of 2 mg/ml MWCNT. Three replications of experiments with hundreds of ion channels presence, P-value < 0.001.

Comparison of the open probability and life-time of channels was shown in Figure 16 and 17. The channel open probability of all levels was significantly lower after adding MWCNT in 1M KCl, and there was a significant decrease for each individual level ($p < 0.001$). Meanwhile, the life-time of the open channels of each level also decreased greatly ($p < 0.001$). The results implied a decrease of open probability and life-time of gA channels that may be caused by MWCNT, which is in agreement with our previous study showing that MWCNT causes the decrease of epinephrine-stimulated secretory Cl^- flux via the CFTR channel [24].

3.3.1.5 MWCNT in DPhPC on gA

The MWCNT was also prepared directly in 2 mg/mL DPhPC in pentane. 10 µl of MWCNT-DPhPC in pentane mixture was added during membrane formation. However, the membrane can never be formed due to some interaction between the MWCNT and DPhPC in the polar solvent.

To study the interaction of MWCNT with DPhPC lipid bilayer, a stable membrane was formed as usual, the gA was added and allowed to form channels and then the MWCNT-DPhPC in pentane mixture was added directly onto the membrane with low volume of 1 µl, which resulted in a MWCNT final concentration of 2 µg/ml. After adding MWCNT-DPhPC in pentane, the well-formed gA channels suddenly dispersed and there were no further channel openings. There was no change in the current baseline or the capacitance of the system. As a control, 1 µl of 2 mg/mL DPhPC in pentane was added to preformed channels. This also caused a significant decrease of open probability to around 0.06, which indicated the disappearance of channels could be related with the DPhPC added rather than the effect of MWCNT. 10 µl of 2 mg/mL DPhPC in pentane was used to form a stable lipid bilayer at the beginning of the experiment. The adding of 1 µl more of 2 mg/mL DPhPC in pentane would cause a 10% increase of the amount of DPhPC and pentane, which may have a drastic effect on the system.

3.3.2 Size measurement of MWCNTs

Figure 18 shows the particle size measurement of different concentrations of MWCNT in the solution of 1M KCl. The particle sizes are found to follow exponential distribution and after log-transformation, the values are normally distributed. With the

low concentration of MWCNT (<0.5 μg/ml), the particle sizes had a median from 1 nm to 10 nm. At a concentration of 5 μg/ml and 50 μg/ml, the particle size had an increase to around 100 nm. With the increase of concentration to 0.5 mg/ml and 5 mg/ml, the particle size kept increasing to around 1400 nm to 2400 nm.

In the solution of 1M KCl, MWCNT cannot be well dispersed and will sediment after some time. In the low concentration, the amount of MWCNT in suspension is limited, which will not have significant effect onto the system. With the increase of concentration, there will be more dispersed MWCNTs that can be detected. These dispersed small-sized MWCNT can interact with cells, which explains why the relatively low concentrations of CNTs have the most toxicity. When the concentration is further increased, the agglomeration of MWCNTs will accelerate the sedimentation of MWCNT, but considerable amount of agglomerated MWCNT are still in suspension in the system, which is captured by the dynamic laser scattering as the large size particles. The particle size of MWCNT is associated with the concentration of MWCNT in the solution, which gives a special aspect of the study of the interaction and function of MWCNT in the system.

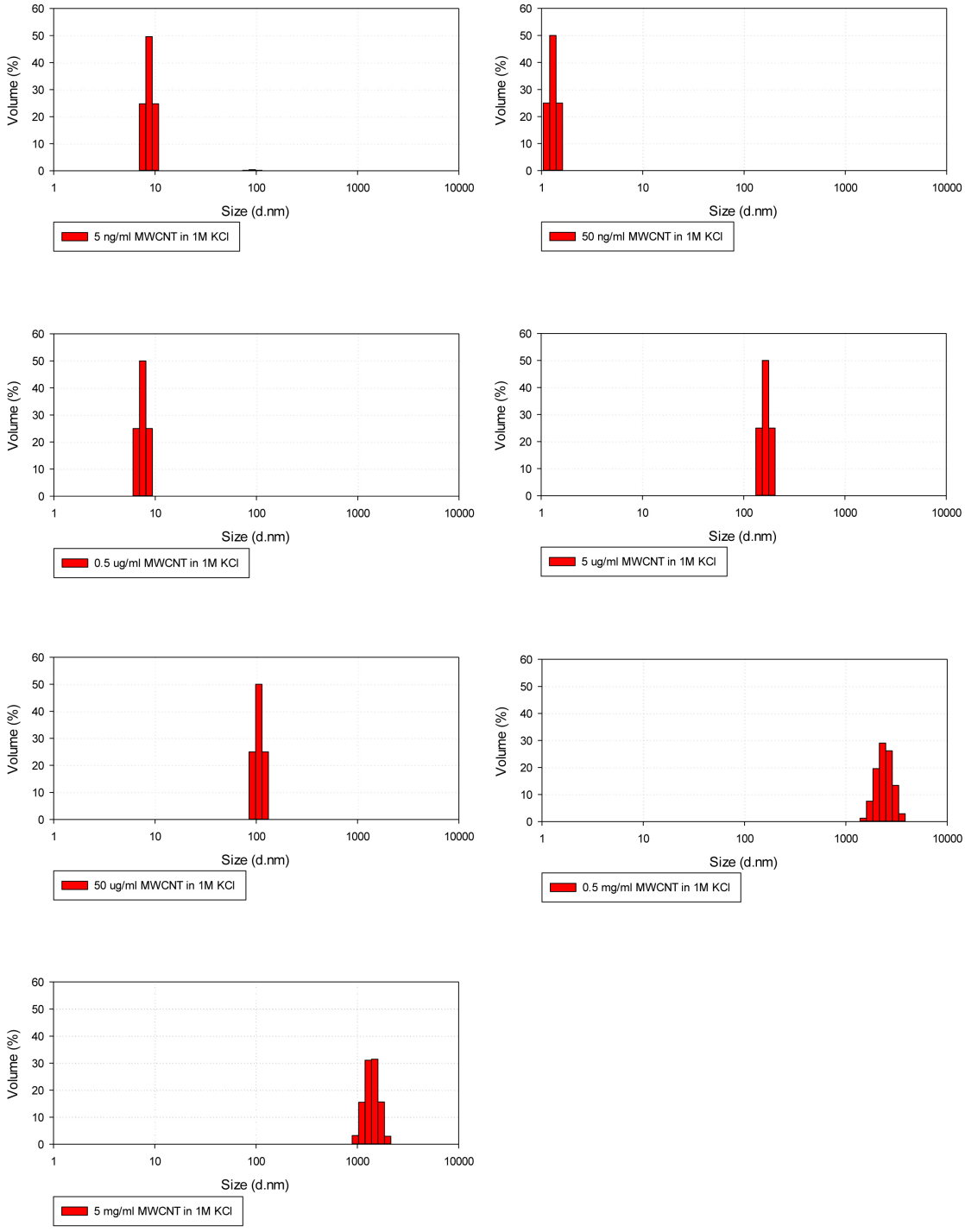

Figure 18 Particle size measurement of short purified MWCNT in 1M KCl with a gradient of concentrations from 5mg/ml to 5ng/ml. The particle sizes were measured by using Zetasizer nano ZS90. The graphs plot size of diameter in nanometer (d.nm) on the X-axis versus volume (%) on the Y-axis. The top line on each Y-axis is 60.

CHAPTER 4. DISCUSSION

Engineered nanoscale materials show a promising future in imaging, electronics and therapeutics. With the spreading applications of nanomaterials, the research of toxic effect on human biological systems has been studied on various levels. Assessment of toxicity has been done on whole animal models, organs, tissues and cell lines with physiology, biochemistry, molecular biology, and proteomics studies. Current research on well-studied nanoparticles such as carbon nanotubes have shown their health effects on the lung including inflammation, interstitial fibrosis and granulomas after exposure by instillation, pharyngeal aspiration and inhalation.

With the development of bioinformatics methods, the effects of different kinds of CNTs on a variety of cell types have been studied on the transcriptomic and proteomic expression level. A proteomics study of 24 h exposure of MWCNT to three cell types representing the most common routes of human exposure to NPs, including macrophage like (THP-1), small airway epithelial (SAE), and intestinal (Caco-2/HT29-MTX) cells found there was no differentially expressed genes or proteins overlapping across all three cell types. The only process significantly regulated in all cell types was related to cell adhesion. In THP-1 cells, MWCNT regulated pathways were involved in increased cell proliferation, DNA repair and anti-apoptosis. The immune response – antigen presentation process was involved in SAE cells after MWCNT exposure [71]. Low

concentration of MWCNT-COOH and MWCNT-PVP exposures to co-cultured intestinal epithelial cells both altered biological function associated to protein synthetic and cell death, but in opposing ways. While MWCNT-COOH exposure down-regulated proteins associated with those two functions as well as carbohydrate metabolism, cell movement, and energy production, MWCNT-PVP exposure revealed increased protein synthetic and cell death, as well as post-translational modification, RNA post-transcriptional modification, and protein folding processes [27].

At high concentration, SWCNT and MWCNT caused an increased nuclear proliferation in renal collecting duct cells mpkCCD$_{cl4}$. At lower, more physiologically relevant concentrations, the CNPs cause changes in epithelial barrier function as well as significant alteration of protein expression and biological function [25]. In our study, the proteomic changes of low concentrations of CNT on airway epithelial cells suggests that several cell functions including cell death and survival, cell-to-cell signaling and interaction, cellular assembly and organization, cellular growth and proliferation, cell movement, infectious disease, molecular transport and protein synthesis are decreased in the cellular response to CNT exposure. The alterations of protein expression associated with biological pathways and functions after CNTs exposure are specific to different cell types, nanotube types and functionalisation as well as concentrations.

Oxidative stress may be one of the mechanisms for toxicity and potential effect demonstrated by the carbon nanotube exposure and a few pathways may be involved. The physicochemical and structural properties of nanoparticle may produce reactive oxygen species (ROS) that can also play important role in the imbalance of prooxidant and antioxidant equilibrium that can result in the oxidative stress [72]. The interaction of

carbon nanotube and cells may have direct effects on the cellular or organelle oxidative status like mitochondrial cell signaling or have indirect effects through inflammatory processes like oxidative burst and phagolysosome activation and enzymatic detoxification pathways [73]. A few proteins and pathways involved in the oxidative stress are identified by our bioinformatics analysis, which is in consistent with this point of view. Through mitochondia-associated antiviral receptor, increased levels of ROS potentiate signaling to activate interferon regulatory factor (IRF)-7 and resulting in an antiviral state, as detected in our proteomic study. The inhibition of methylglyoxal degradation indicates the detoxification pathways are also involved in the oxidative status in response to CNT exposure.

After 24h exposure to CNT, Calu-3 cells are found to have an increase of function of cell death. Compared to the 'self-killing' apoptosis of programmed cell death, the 'self-eating' autophagy can be a stress adaptation that avoids cell death which suppresses apoptosis, or an alternative cell-death pathway under some circumstances [74]. It is reported that functionalized SWCNT could induce autophagic cell death in human lung adenocarcinoma A549 cells and cause acute lung injury in mice [75]. Without any detected evidence for apoptosis, the COOH-CNT induced A549 cell death was thought to follow autophagy by other pathways including AKT–TSC2–mTOR signaling pathway. The *in vivo* study also revealed that an autophagy inhibitor could ameliorate acute lung injury induced by COOH-CNT, which indicates the important role of autophagy in COOH-CNT-induced acute lung toxicity in mice. While these kinases such as mTOR, PI3K and AMPK directly regulate autophagy, other kinases such as mitogen-activated protein kinase (MAPK) and protein kinase C (PKC) are also involved by indirectly

regulation of the function and levels of proteins related to autophagy. The activation of MAPK, which is detected in our proteomics studies, lead to phosphorylation-dependent activation of other kinases and transcription factors [76]. These factors such as e extracellular signal-regulated kinase (ERK)/mitogen-activated protein kinase (MAPK), p38, c-Jun N-terminal kinase (JNK)/stress-activated protein kinase (SAPK) are shown to positively or negatively regulate autophagy in different cells under different circumstances. In our research, the activation of MAPK in Calu-3 cells after exposure to CNT is in coincidence with the increase of cell function of cell death, which indicates the probable role of autophagy in cells under stress. The autophagy provides another pathway resulting in loss of cell viability after CNT exposure, which gives a new clue to study the toxicity of CNT on cells.

To cause biological effects, carbon nanotubes must interface with cell membranes and the mechanism of how carbon nanotubes enter cells remains unclear. The approach and attachment of carbon nanotube to the membrane surface is an important step towards the uptake and penetration of carbon nanotubes. Artificial lipid models and computer simulations shed light on the biophysics study of CNT-membrane interaction. Some favorable conditions like cations and pH are found to increase the deposition of MWCNTs on DOPC vesicles [77]. Simulations indicated that CNTs with closed, rounded end caps at their tips can initiate uptake by tip recognition through receptor binding and rotation driven by asymmetric elastic strain at the tube–bilayer interface, and have a near-vertical entry with the minimized membrane elastic energy. Nanotubes without caps at the end showed a different mode of membrane interaction by sinking into the membrane [61]. The CNTs in our study are originally capped with fullerenic hemispheres during the

manufacturing process, but sonication when preparing CNTs for cell treatment may break the CNTs with high aspect ratio and left opened fractions. The agglomeration further increases the complexity of the structure of CNT bundles.

There are a few hypotheses of the mechanism of cell entry of CNT, which have not been confirmed yet. Shi et al. showed field-emission SEM images as experimental evidence for tip-entry of MWCNTs with cell membrane invagination at the point of entry [61]. Reduced MWCNT uptake at 4 ℃ and in the presence of a metabolic inhibitor mixture containing NaF, NaN3 and antimycin A indicated this tip-entry is by means of energy-dependent endocytosis. Research by Yaron et al. showed that pluronic-stabilized SWCNTs associated with membranes but did not possess sufficient insertion energy to penetrate the membrane, which also indicated that SWCNTs enter cells by endocytosis instead of penetration [78]. On the contrary, Corredora et al. observed a significant transmembrane current fluxes induced by functionalized MWCNTs by electrophysiological measurements. This is in favor of the penetration of MWCNTs that can form transmembrane channels and allow the ion flux [79]. In our ion channel measurement, there is no detectable current flux that could be characterized as ion transport according to MWCNT penetration, which doesn't back up the model of penetration. More experimental evidence of the interaction of non-functionalized CNT with membrane is needed to solve the controversy and clarify the mechanism of cell entry.

Located in the lipid bilayer, integral membrane protein function may be regulated by the composition of host lipid bilayer. Changes in bilayer physical properties can result in the alteration of membrane protein function. The presence of the nanotubes can reduce the mobility of lipid molecules within the membrane and even cause a phase change that

can reconstruct the lipid [62,65]. These changes could have an effect on the association and disassociation of the gA monomers inserted into the lipid bilayer. This could be responsible for the change of the open and close times of gA channels that were measured in our ion channel studies.

The documented decrease of lifetime and open probability of gA channels could result from interactions of CNT with lipid bilayer, or on the other hand, from the direct interactions with ion channels. The method of whole-cell patch clamp is widely used to study the effect of CNT on different ion channels on several kinds of cells and provided valuable channel activity data. Work by Park et al. has indicated that SWCNTs are a new kind of ion channel blockers and have a significant effect on varieties of K^+ channels including Caenorhabditis elegans EXP-2, KVS-1, human KCNQ1, Kv4.2 and HERG potassium channels on Chinese hamster ovary (CHO) cells as reflected by the whole-cell patch clamp recordings [80]. With conserved three-dimensional structure of the pores, these phylogenetically distant K^+ channels are all susceptible to nanotubes. The blockage was dependent on the dose as well as shape and dimensions of the nanoparticles and through a pore occlusion mechanism that did not require any electrochemical interaction. Besides, CNTs are also found to block mechano-sensitive ion channels by interacting with extracellular domain [81]. Instead of direct structural interaction, CNTs can also cause an inhibition of neuronal voltage-gated calcium ion channels by releasing yttrium (Y) [82]. Yttrium (Y) is commonly used as a catalyst for nanotube growth and may have some residues left after manufacturing process. The mechanism of yttrium as a channel blocker is because of the strong binding of yttrium and carboxylate, and this competitively binding can displace calcium ions from their binding sites within the ion

channel and resulted as a decrease of the whole cell patch clamp current. Claimed as purified, the CNTs used in our study don't have detectable levels of Yttrium (Y), but they still have measureable levels of iron (Fe), nickel (Ni) and/or cobalt (Co) together with less than 5% of the total weight, which may have effect on ion channels and cells [25]. However, the substantial dilution of CNT preparation makes this unlikely.

As characterized by dynamic light scattering, the average size of CNTs is in a larger scale compared with the dimension of gA channels, but there may still exist some CNT fragments with size small enough that could have structural interaction with gA channels. We are the first to find the decrease of the lifetime and open probability of gA channels after CNT exposure by single channel recording and analysis, and further research needs to be done to clarify the change of ion channel activities. This suggests new uses for CNTs in biological applications and provide insights into the current view of mechanisms of the interaction of CNT with proteins.

Mimicking cell membrane, the model membrane study provides fundamental biophysical insight into the CNT-membrane interaction and helps to explain physiological responses. However, in cell membranes, the composition and diversity are more complicated than in the homogenous model membrane. How to extend the understanding of interaction of CNT with model membrane to the real membrane remains to be elucidated. In addition, because of the manufacturing technique and process, there is an inevitably lack of homogeneity of the CNT as shown by the size characterization by Dynamic Light Scattering. With a wide range of size and mass, it is important to understand which type of CNTs is responsible for the detected effect and further the study by CNT purification. There is still a long but interesting way to go to determine the

possible mechanisms of the interaction of carbon nanotube with cell membrane and nanotoxicity of carbon nanotube to cells.

CHAPTER 5. CONCLUSIONS

Bioinformatic analysis of proteomic changes that occur in Calu-3 in response to exposure to carbon nanotubes shows there are many proteins and cellular functions that change in response to low, but not high, levels of exposure to CNTs. The overlap in the nature of the proteins that are altered in response to low levels exposure of both single wall and multiwall carbon nanotubes is surprising and underscores the validity of the analyses as to which proteins play important roles in the cell response to carbon nanotubes. The short MWCNT cause a decrease of the open probability and lifetime of gA channels, which suggests that the nanotubes can interact with the lipid membrane and channel proteins. This may contribute to their effects on ion transport and biological processes. These studies help to highlight the potential toxic effects of nanomaterials to human health.

BIBLIOGRAPHY

BIBLIOGRAPHY

1. Ferrari, M., Cancer nanotechnology: Opportunities and challenges. *Nature Reviews Cancer* **2005**, *5*, 161-171.
2. Peer, D.; Karp, J.M.; Hong, S.; Farokhzad, O.C.; Margalit, R.; Langer, R., Nanocarriers as an emerging platform for cancer therapy. *Nature Nanotechnology* **2007**, *2*, 751-760.
3. Kircher, M.F.; Mahmood, U.; King, R.S.; Weissleder, R.; Josephson, L., A multimodal nanoparticle for preoperative magnetic resonance imaging and intraoperative optical brain tumor delineation. *Cancer Research* **2003**, *63*, 8122-8125.
4. Cheng, M.M.-C.; Cuda, G.; Bunimovich, Y.L.; Gaspari, M.; Heath, J.R.; Hill, H.D.; Mirkin, C.A.; Nijdam, A.J.; Terracciano, R.; Thundat, T., Nanotechnologies for biomolecular detection and medical diagnostics. *Current Opinion in Chemical Biology* **2006**, *10*, 11-19.
5. NNI, National nanotechnology initiative supplement to the presiden's 2014 budget. 2014.
6. Oberdörster, G.; Oberdörster, E.; Oberdörster, J., Nanotoxicology: An emerging discipline evolving from studies of ultrafine particles. *Environmental Health Perspectives* **2005**, *113*, 823.

7. Krug, H.F.; Wick, P., Nanotoxicology: An interdisciplinary challenge. *Angewandte Chemie International Edition* **2011**, *50*, 1260-1278.

8. Buzea, C.; Pacheco, II; Robbie, K., Nanomaterials and nanoparticles: Sources and toxicity. *Biointerphases* **2007**, *2*, MR17-71.

9. Moghimi, S.M.; Hunter, A.C.; Murray, J.C., Nanomedicine: Current status and future prospects. *The FASEB Journal* **2005**, *19*, 311-330.

10. Iijima, S., Helical microtubules of graphitic carbon. *Nature* **1991**, *354*, 56-58.

11. De Volder, M.F.; Tawfick, S.H.; Baughman, R.H.; Hart, A.J., Carbon nanotubes: Present and future commercial applications. *Science* **2013**, *339*, 535-539.

12. Smart, S.; Cassady, A.; Lu, G.; Martin, D., The biocompatibility of carbon nanotubes. *Carbon* **2006**, *44*, 1034-1047.

13. Chen, R.J.; Bangsaruntip, S.; Drouvalakis, K.A.; Kam, N.W.S.; Shim, M.; Li, Y.; Kim, W.; Utz, P.J.; Dai, H., Noncovalent functionalization of carbon nanotubes for highly specific electronic biosensors. *Proceedings of the National Academy of Sciences* **2003**, *100*, 4984-4989.

14. Klumpp, C.; Kostarelos, K.; Prato, M.; Bianco, A., Functionalized carbon nanotubes as emerging nanovectors for the delivery of therapeutics. *Biochimica et Biophysica Acta (BBA)-Biomembranes* **2006**, *1758*, 404-412.

15. Wong Shi Kam, N.; Dai, H., Single walled carbon nanotubes for transport and delivery of biological cargos. *Physica Status Solidi (b)* **2006**, *243*, 3561-3566.

16. Correa-Duarte, M.A.; Wagner, N.; Rojas-Chapana, J.; Morsczeck, C.; Thie, M.; Giersig, M., Fabrication and biocompatibility of carbon nanotube-based 3d networks as scaffolds for cell seeding and growth. *Nano Letters* **2004**, *4*, 2233-2236.

17. Zanello, L.P.; Zhao, B.; Hu, H.; Haddon, R.C., Bone cell proliferation on carbon nanotubes. *Nano Letters* **2006**, *6*, 562-567.

18. Cui, H.F.; Vashist, S.K.; Al-Rubeaan, K.; Luong, J.H.; Sheu, F.S., Interfacing carbon nanotubes with living mammalian cells and cytotoxicity issues. *Chemical Research in Toxicology* **2010**, *23*, 1131-1147.

19. Poland, C.A.; Duffin, R.; Kinloch, I.; Maynard, A.; Wallace, W.A.; Seaton, A.; Stone, V.; Brown, S.; MacNee, W.; Donaldson, K., Carbon nanotubes introduced into the abdominal cavity of mice show asbestos-like pathogenicity in a pilot study. *Nature Nanotechnology* **2008**, *3*, 423-428.

20. Lam, C.-W.; James, J.T.; McCluskey, R.; Hunter, R.L., Pulmonary toxicity of single-wall carbon nanotubes in mice 7 and 90 days after intratracheal instillation. *Toxicological Sciences* **2004**, *77*, 126-134.

21. Muller, J.; Huaux, F.; Moreau, N.; Misson, P.; Heilier, J.F.; Delos, M.; Arras, M.; Fonseca, A.; Nagy, J.B.; Lison, D., Respiratory toxicity of multi-wall carbon nanotubes. *Toxicology and Applied Pharmacology* **2005**, *207*, 221-231.

22. Zhu, Y.; Chidekel, A.; Shaffer, T.H., Cultured human airway epithelial cells (calu-3): A model of human respiratory function, structure, and inflammatory responses. *Critical Care Research and Practice* **2010**, *2010*.

23. Powell, D.W., Barrier function of epithelia. *The American Journal of Physiology* **1981**, *241*, G275-288.

24. Banga, A.; Witzmann, F.A.; Petrache, H.I.; Blazer-Yost, B.L., Functional effects of nanoparticle exposure on calu-3 airway epithelial cells. *Cellular Physiology and Biochemistry* **2012**, *29*, 197-212.

25. Blazer-Yost, B.L.; Banga, A.; Amos, A.; Chernoff, E.; Lai, X.; Li, C.; Mitra, S.; Witzmann, F.A., Effect of carbon nanoparticles on renal epithelial cell structure, barrier function, and protein expression. *Nanotoxicology* **2011**, *5*, 354-371.

26. Prince, K.L.; Colvin, S.C.; Park, S.; Lai, X.; Witzmann, F.A.; Rhodes, S.J., Developmental analysis and influence of genetic background on the lhx3 w227ter mouse model of combined pituitary hormone deficiency disease. *Endocrinology* **2013**, *154*, 738-748.

27. Lai, X.; Blazer–Yost, B.L.; Clack, J.W.; Fears, S.L.; Mitra, S.; Ntim, S.A.; Ringham, H.N.; Witzmann, F.A., Protein expression profiles of intestinal epithelial co–cultures: Effect of functionalised carbon nanotube exposure. *International Journal of Biomedical Nanoscience and Nanotechnology* **2013**, *3*, 127-162.

28. Lai, X.; Agarwal, M.; Lvov, Y.M.; Pachpande, C.; Varahramyan, K.; Witzmann, F.A., Proteomic profiling of halloysite clay nanotube exposure in intestinal cell co‐culture. *Journal of Applied Toxicology* **2013**.

29. Vidanapathirana, A.K.; Lai, X.; Hilderbrand, S.C.; Pitzer, J.E.; Podila, R.; Sumner, S.J.; Fennell, T.R.; Wingard, C.J.; Witzmann, F.A.; Brown, J.M., Multi-walled carbon nanotube directed gene and protein expression in cultured human aortic endothelial cells is influenced by suspension medium. *Toxicology* **2012**, *302*, 114-122.

30. Lai, X.; Bacallao, R.L.; Blazer-Yost, B.L.; Hong, D.; Mason, S.B.; Witzmann, F.A., Characterization of the renal cyst fluid proteome in autosomal dominant polycystic kidney disease (adpkd) patients. *Proteomics. Clinical Applications* **2008**, *2*, 1140-1152.

31. Keller, A.; Nesvizhskii, A.I.; Kolker, E.; Aebersold, R., Empirical statistical model to estimate the accuracy of peptide identifications made by ms/ms and database search. *Analytical Chemistry* **2002**, *74*, 5383-5392.

32. Nesvizhskii, A.I.; Keller, A.; Kolker, E.; Aebersold, R., A statistical model for identifying proteins by tandem mass spectrometry. *Analytical Chemistry* **2003**, *75*, 4646-4658.

33. Seattle proteome center (spc). The trans-proteomic pipeline (tpp, v. 3.3.0). Available online: Http://tools.Proteomecenter.Org/software.Php (accessed on July 25, 2013)

34. Lai, X.; Wang, L.; Tang, H.; Witzmann, F.A., A novel alignment method and multiple filters for exclusion of unqualified peptides to enhance label-free quantification using peptide intensity in lc-ms/ms. *Journal of Proteome Research* **2011**, *10*, 4799-4812.

35. Monroe, M.E.; Shaw, J.L.; Daly, D.S.; Adkins, J.N.; Smith, R.D., Masic: A software program for fast quantitation and flexible visualization of chromatographic profiles from detected lc-ms(/ms) features. *Computational Biology and Chemistry* **2008**, *32*, 215-217.

36. Storey, J.D., A direct approach to false discovery rates. *Journal of the Royal Statistical Society: Series B (Statistical Methodology)* **2002**, *64*, 479-498.

37. Ingenuity systems. The ingenuity pathway analysis (ipa) web based software. Available online: Http://www.Ingenuity.Com (accessed on September 23, 2013).

38. String. Available online: Http://string-db.Org/ (accessed on March 3, 2013).

39. Szklarczyk, D.; Franceschini, A.; Kuhn, M.; Simonovic, M.; Roth, A.; Minguez, P.; Doerks, T.; Stark, M.; Muller, J.; Bork, P.*, et al.*, The string database in 2011: Functional interaction networks of proteins, globally integrated and scored. *Nucleic Acids Research* **2011**, *39*, D561-568.

40. Oberdorster, G.; Oberdorster, E.; Oberdorster, J., Nanotoxicology: An emerging discipline evolving from studies of ultrafine particles. *Environmental Health Perspectives* **2005**, *113*, 823-839.

41. Ge, C.; Du, J.; Zhao, L.; Wang, L.; Liu, Y.; Li, D.; Yang, Y.; Zhou, R.; Zhao, Y.; Chai, Z.*, et al.*, Binding of blood proteins to carbon nanotubes reduces cytotoxicity. *Proceedings of the National Academy of Sciences of the United States of America* **2011**, *108*, 16968-16973.

42. Shannahan, J.H.; Brown, J.M.; Chen, R.; Ke, P.C.; Lai, X.; Mitra, S.; Witzmann, F.A., Comparison of nanotube–protein corona composition in cell culture media. *Small* **2013**.

43. Monopoli, M.P.; Åberg, C.; Salvati, A.; Dawson, K.A., Biomolecular coronas provide the biological identity of nanosized materials. *Nature Nanotechnology* **2012**, *7*, 779-786.

44. Kam, N.W.; Dai, H., Carbon nanotubes as intracellular protein transporters: Generality and biological functionality. *Journal of the American Chemical Society* **2005**, *127*, 6021-6026.

45. Fett, R.; Knippers, R., The primary structure of human glutaminyl-trna synthetase. A highly conserved core, amino acid repeat regions, and homologies with translation elongation factors. *Journal of Biological Chemistry* **1991**, *266*, 1448-1455.

46. Rollins, B.M.; Burn, M.; Coakley, R.D.; Chambers, L.A.; Hirsh, A.J.; Clunes, M.T.; Lethem, M.I.; Donaldson, S.H.; Tarran, R., A2b adenosine receptors regulate the mucus clearance component of the lung's innate defense system. *American Journal of Respiratory Cell and Molecular Biology* **2008**, *39*, 190-197.

47. Kawkitinarong, K.; Linz-McGillem, L.; Birukov, K.G.; Garcia, J.G., Differential regulation of human lung epithelial and endothelial barrier function by thrombin. *American Journal of Respiratory Cell and Molecular Biology* **2004**, *31*, 517-527.

48. Weis, K., Importins and exportins: How to get in and out of the nucleus. *Trends in Biochemical Sciences* **1998**, *23*, 185-189.

49. Lee, J.C.; Jong, H.S.; Yoo, C.G.; Han, S.K.; Shim, Y.S.; Kim, Y.W., Telomerase activity in lung cancer cell lines and tissues. *Lung Cancer* **1998**, *21*, 99-103.

50. Chen, Y.; Qu, K.; Zhao, C.; Wu, L.; Ren, J.; Wang, J.; Qu, X., Insights into the biomedical effects of carboxylated single-wall carbon nanotubes on telomerase and telomeres. *Nature Communications* **2012**, *3*, 1074.

51. Kultz, D., Molecular and evolutionary basis of the cellular stress response. *Annual Review of Physiology* **2005**, *67*, 225-257.

52. Holt, B.D.; Short, P.A.; Rape, A.D.; Wang, Y.L.; Islam, M.F.; Dahl, K.N., Carbon nanotubes reorganize actin structures in cells and ex vivo. *ACS Nano* **2010**, *4*, 4872-4878.

53. Zahm, J.M.; Kaplan, H.; Herard, A.L.; Doriot, F.; Pierrot, D.; Somelette, P.; Puchelle, E., Cell migration and proliferation during the in vitro wound repair of the respiratory epithelium. *Cell Motility and the Cytoskeleton* **1997**, *37*, 33-43.

54. Chun, J.; Prince, A., Tlr2-induced calpain cleavage of epithelial junctional proteins facilitates leukocyte transmigration. *Cell Host & Microbe* **2009**, *5*, 47-58.

55. Chin, J.E.; Hatfield, C.A.; Winterrowd, G.E.; Brashler, J.R.; Vonderfecht, S.L.; Fidler, S.F.; Griffin, R.L.; Kolbasa, K.P.; Krzesicki, R.F.; Sly, L.M.*, et al.*, Airway recruitment of leukocytes in mice is dependent on alpha4-integrins and vascular cell adhesion molecule-1. *The American Journal of Physiology* **1997**, *272*, L219-229.

56. Hudder, A.; Nathanson, L.; Deutscher, M.P., Organization of mammalian cytoplasm. *Molecular and Cellular Biology* **2003**, *23*, 9318-9326.

57. BARABÁSI, B.A.-L.; Bonabeau, E., Scale-free. *Scientific American* **2003**.

58. Delprato, A., Topological and functional properties of the small gtpases protein interaction network. *PloS One* **2012**, *7*, e44882.

59. Fievet, B.; Louvard, D.; Arpin, M., Erm proteins in epithelial cell organization and functions. *Biochimica et Biophysica acta* **2007**, *1773*, 653-660.

60. Srinivasula, S.M.; Poyet, J.L.; Razmara, M.; Datta, P.; Zhang, Z.; Alnemri, E.S., The pyrin-card protein asc is an activating adaptor for caspase-1. *The Journal of Biological Chemistry* **2002**, *277*, 21119-21122.

61. Shi, X.; von dem Bussche, A.; Hurt, R.H.; Kane, A.B.; Gao, H., Cell entry of one-dimensional nanomaterials occurs by tip recognition and rotation. *Nature Nanotechnology* **2011**, *6*, 714-719.

62. Dawson, K.A.; Salvati, A.; Lynch, I., Nanotoxicology: Nanoparticles reconstruct lipids. *Nature Nanotechnology* **2009**, *4*, 84-85.

63. Li, P.; Lai, X.; Witzmann, F.A.; Blazer-Yost, B.L., Bioinformatic analysis of differential protein expression in calu-3 cells exposed to carbon nanotubes. *Proteomes* **2013**, *1*, 219-239.

64. Mueller, P.; Rudin, D.O.; Ti Tien, H.; Wescott, W.C., Reconstitution of cell membrane structure in vitro and its transformation into an excitable system. *Nature* **1962**, *194*, 979-980.

65. Parthasarathi, R.; Tummala, N.R.; Striolo, A., Embedded single-walled carbon nanotubes locally perturb dopc phospholipid bilayers. *The Journal of Physical Chemistry. B* **2012**, *116*, 12769-12782.

66. Kelkar, D.A.; Chattopadhyay, A., The gramicidin ion channel: A model membrane protein. *Biochimica et Biophysica Acta (BBA)-Biomembranes* **2007**, *1768*, 2011-2025.

67. O'Connell, A.M.; Koeppe, R.E.; Andersen, O.S., Kinetics of gramicidin channel formation in lipid bilayers: Transmembrane monomer association. *Science* **1990**, *250*, 1256-1259.

68. Millhauser, G.L.; Salpeter, E.E.; Oswald, R.E., Diffusion models of ion-channel gating and the origin of power-law distributions from single-channel recording. *Proceedings of the National Academy of Sciences* **1988**, *85*, 1503-1507.

69. Hladky, S.; Haydon, D., Ion transfer across lipid membranes in the presence of gramicidin a: I. Studies of the unit conductance channel. *Biochimica et Biophysica Acta (BBA)-Biomembranes* **1972**, *274*, 294-312.

70. Jochems, C.E.; van der Valk, J.B.; Stafleu, F.R.; Baumans, V., The use of fetal bovine serum: Ethical or scientific problem? *ATLA-NOTTINGHAM-* **2002**, *30*, 219-228.

71. Tilton, S.C.; Karin, N.; Tolic, A.; Xie, Y.; Lai, X.; Hamilton, R.F.; Waters, K.; Holian, A.; Witzmann, F.A.; Orr, G., Three human cell types respond to multi-walled carbon nanotubes and titanium dioxide nanobelts with cell-specific transcriptomic and proteomic expression patterns. *Nanotoxicology* **2013**, 1-40.

72. Nel, A.; Xia, T.; Mädler, L.; Li, N., Toxic potential of materials at the nanolevel. *Science* **2006**, *311*, 622-627.

73. Madl, A.K.; Plummer, L.E.; Carosino, C.; Pinkerton, K.E., Nanoparticles, lung injury, and the role of oxidant stress. *Annual Review of Physiology* **2013**.

74. Maiuri, M.C.; Zalckvar, E.; Kimchi, A.; Kroemer, G., Self-eating and self-killing: Crosstalk between autophagy and apoptosis. *Nature Reviews Molecular Cell Biology* **2007**, *8*, 741-752.

75. Liu, H.; Zhang, Y.; Yang, N.; Zhang, Y.; Liu, X.; Li, C.; Zhao, Y.; Wang, Y.; Zhang, G.; Yang, P., A functionalized single-walled carbon nanotube-induced autophagic cell death in human lung cells through akt–tsc2-mtor signaling. *Cell Death & Disease* **2011**, *2*, e159.

76. Sridharan, S.; Jain, K.; Basu, A., Regulation of autophagy by kinases. *Cancers* **2011**, *3*, 2630-2654.

77. Yi, P.; Chen, K.L., Interaction of multiwalled carbon nanotubes with supported lipid bilayers and vesicles as model biological membranes. *Environmental Science & Technology* **2013**, *47*, 5711-5719.

78. Yaron, P.N.; Holt, B.D.; Short, P.A.; Losche, M.; Islam, M.F.; Dahl, K.N., Single wall carbon nanotubes enter cells by endocytosis and not membrane penetration. *J Nanobiotechnology* **2011**, *9*, 45.

79. Corredor, C.; Hou, W.-C.; Klein, S.A.; Moghadam, B.Y.; Goryll, M.; Doudrick, K.; Westerhoff, P.; Posner, J.D., Disruption of model cell membranes by carbon nanotubes. *Carbon* **2013**, *60*, 67-75.

80. Park, K.H.; Chhowalla, M.; Iqbal, Z.; Sesti, F., Single-walled carbon nanotubes are a new class of ion channel blockers. *Journal of Biological Chemistry* **2003**, *278*, 50212-50216.

81. Patel, A.; Smita, S.; Rahman, Q.; Gupta, S.K.; Verma, M.K., Single wall carbon nanotubes block ion passage in mechano-sensitive ion channels by interacting with extracellular domain. *Journal of Biomedical Nanotechnology* **2011**, *7*, 183-185.

82. Jakubek, L.M.; Marangoudakis, S.; Raingo, J.; Liu, X.; Lipscombe, D.; Hurt, R.H., The inhibition of neuronal calcium ion channels by trace levels of yttrium released from carbon nanotubes. *Biomaterials* **2009**, *30*, 6351-6357.

PUBLICATIONS

PUBLICATIONS

Proteomes **2013**, *1*, 219-239; doi:10.3390/proteomes1030219

OPEN ACCESS

proteomes

ISSN 2227-7382

www.mdpi.com/journal/proteomes

Article

Bioinformatic Analysis of Differential Protein Expression in Calu-3 Cells Exposed to Carbon Nanotubes

Pin Li [1], Xianyin Lai [2], Frank A. Witzmann [2] and Bonnie L. Blazer-Yost [1,2,*]

[1] Department of Biology, Indiana University Purdue University, 723 West Michigan Street, Indianapolis, IN 46202, USA; E-Mail: lipin@iupui.edu

[2] Department of Cellular and Integrative Physiology, Indiana University School of Medicine, 1345 West 16th Street, Indianapolis, IN 46202, USA; E-Mails: xlai@iupui.edu (X.L.); fwitzman@iu.edu (F.A.W.)

* Author to whom correspondence should be addressed; E-Mail: bblazer@iupui.edu; Tel.: +1-317-278-1145; Fax: +1-317-274-2846.

Received: 26 July 2013; in revised form: 29 September 2013 / Accepted: 30 September 2013 / Published: 14 October 2013

Abstract: Carbon nanomaterials are widely produced and used in industry, medicine and scientific research. To examine the impact of exposure to nanoparticles on human health, the human airway epithelial cell line, Calu-3, was used to evaluate changes in the cellular proteome that could account for alterations in cellular function of airway epithelia after 24 hexposure to 10 μg/mL and 100 ng/mLof two common carbon nanoparticles, single- and multi-wall carbon nanotubes (SWCNT, MWCNT). After exposure to the nanoparticles, label-free quantitative mass spectrometry (LFQMS) was used to study the differential protein expression. Ingenuity Pathway Analysis (IPA) was used to conduct a bioinformaticanalysis of proteins identified in LFQMS. Interestingly, after exposure to ahigh concentration (10 μg/mL; 0.4 μg/cm^2) of MWCNT or SWCNT, only 8 and 13 proteins, respectively, exhibited changes in abundance. In contrast, the abundance of hundreds of proteins was altered in response to a low concentration (100 ng/mL; 4 ng/cm^2) of either CNT. Of the 281 and 282 proteins that were significantly altered in response to MWCNT or SWCNT respectively, 231 proteins were the same. Bioinformatic analyses found that the proteins in common to both nanotubes occurred within the cellular functions of cell death and survival, cell-to-cell signaling and interaction, cellular assembly and organization, cellular growth and proliferation, infectious disease, molecular transport and protein synthesis. The majority of the protein changes represent a decrease in amount suggesting a general stress response to protect cells. The STRING database was used to analyze the